

**NASA CONTRACTOR
REPORT**

NASA CR-1853



NASA CR-1853
C.1

0061025



TECH LIBRARY KAFB, NM

**LOAN COPY: RETURN TO
AFWL (DO/L)
KIRTLAND AFB, N. M.**

**STUDY AND DEVELOPMENT
OF ACOUSTIC TREATMENT
FOR JET ENGINE TAILPIPES**

*by M. D. Nelsen, L. L. Linscheid, B. A. Dinwiddie III,
and O. J. Hall, Jr.*

Prepared by
THE BOEING COMPANY
Wichita, Kans. 67210
for Langley Research Center

NATIONAL AERONAUTICS AND SPACE ADMINISTRATION • WASHINGTON, D. C. • NOVEMBER 1971



0061025

1. Report No. NASA CR-1853	2. Government Accession No.	3. Recipient's Catalog No.	
4. Title and Subtitle Study and Development of Acoustic Treatment for Jet Engine Tailpipes		5. Report Date November 1971	6. Performing Organization Code
		8. Performing Organization Report No. D3-8535	10. Work Unit No.
7. Author(s) M. D. Nelsen, L. L. Linscheid, B. A. Dinwiddie III, and O. J. Hall, Jr.		11. Contract or Grant No. NAS1-9622	13. Type of Report and Period Covered Contractor Report
9. Performing Organization Name and Address The Boeing Company Wichita Division Wichita, Kansas		14. Sponsoring Agency Code	
		12. Sponsoring Agency Name and Address National Aeronautics and Space Administration Washington, D.C. 20546	
15. Supplementary Notes			
16. Abstract <p>A study and development program was accomplished to attenuate turbine noise generated in the JT3D turbofan engine. Analytical studies were used to design an acoustic liner for the tailpipe. Engine ground tests defined the tailpipe environmental factors and laboratory tests were used to support the analytical studies.</p> <p>Furnace-brazed, stainless steel, perforated sheet acoustic liners were designed, fabricated, installed, and ground tested in the tailpipe of a JT3D engine. Test results showed the turbine tones were suppressed below the level of the jet exhaust for most far field polar angles.</p>			
17. Key Words (Suggested by Author(s)) Noise, aircraft Material, acoustic 707, airplane Acoustic treatment, tailpipes Economics		18. Distribution Statement Unclassified - Unlimited	
19. Security Classif. (of this report) Unclassified	20. Security Classif. (of this page) Unclassified	21. No. of Pages 66	22. Price* \$3.00

CONTENTS

	<u>Page</u>
SUMMARY	1
INTRODUCTION	2
SYMBOLS	3
SUPPRESSOR DESIGN STUDIES	5
Tailpipe Internal Survey Tests	5
Test installation and instrumentation	5
Results	7
Suppressor Configuration Trades	8
Suppressor Development	9
Acoustic panel construction	10
Lining placement and geometry	10
Acoustic performance verification tests	11
Full scale suppressor	12
FULL SCALE TESTS	13
Test Installation and Instrumentation	13
Results	13
ECONOMIC STUDIES	16
CONCLUDING REMARKS	17
APPENDIX	19
REFERENCES	27

FIGURES

<u>No.</u>	<u>Title</u>	<u>Page</u>
1	NASA quiet nacelle	28
2	Maximum fan exhaust noise at approach power, ground test	28
3	Engine test installation	29
4	Aeroacoustic instrumentation, baseline tailpipe	30
5	Tailpipe internal survey traversing probe assembly	31
6	Schematic of traversing probe assembly	31
7	Aeroacoustic traversing probe details	32
8	Tailpipe internal survey instrumentation	33
9	Velocity survey, baseline tailpipe	34
10	Total temperature survey, baseline tailpipe	35
11	Acoustic survey, baseline tailpipe	36
12	Fourth stage turbine tone survey	37
13	Tailpipe lining concepts	38
14	Single-ring treated tailpipe assembly	39
15	Typical perforated sheet acoustic panel	40
16	Predicted attenuation for perforated sheet lining	41
17	Flow duct configurations	42
18	Flow duct turbine tone simulation	43
19	Flow duct acoustic panels installed	43
20	Flow duct noise spectra, simulated turbine tone	44
21	Comparison of analytical predictions with flow duct test results	45
22	Flow duct random noise attenuation	45

FIGURES (Continued)

<u>No.</u>	<u>Title</u>	<u>Page</u>
23	Treated tailpipe assembly	46
24	Furnace-brazed, stainless steel, acoustic panels	46
25	NASA flightworthy quiet nacelle installed on JT3D-3B engine	47
26	Far field microphone polar array	47
27	Treated tailpipe installation	48
28	Effect of treated tailpipe on engine thrust	49
29	Far field noise spectra from ground microphone	50
30	Far field noise spectra from engine G_L microphone	51
31	Microphone height effect on 4th stage turbine tone measurements	52
32	Comparison of 2nd and 4th stage turbine tone suppression	52
33	Effect of higher approach power conditions on 4th stage turbine tone suppression	53
34	Tailpipe noise comparison at approach power	54
35	Perceived noise time history during landing approach	54
36	NASA quiet nacelle average price comparison	55
37	Acoustic lining design analysis procedure	56
38	Geometry of duct	57
39	Optimum admittance determination	57
40	Optimization of acoustic ring placement	58
41	Face sheet blockage trades based on design frequency	59
42	Face sheet blockage trades based on peak attenuation frequency	60

FIGURES (Continued)

<u>No.</u>	<u>Title</u>	<u>Page</u>
43	Core depth variation trades based on design frequency	61
44	Core depth variation trades based on peak attenuation frequency	62

TABLES

<u>No.</u>	<u>Title</u>	<u>Page</u>
I	Tailpipe trade study summary	9
II	Perforated sheet acoustic lining data	12
III	DOC increase over flightworthy quiet nacelle	16

STUDY AND DEVELOPMENT OF ACOUSTIC TREATMENT FOR JET ENGINE TAILPIPES

By M. D. Nelsen, L. L. Linscheid, B. A. Dinwiddie III, and O. J. Hall, Jr.
The Boeing Company

SUMMARY

An acoustically treated tailpipe was designed, fabricated, and ground tested on a JT3D turbofan engine. The tailpipe was designed to reduce the turbine noise emanating from the engine to a level below that of the jet exhaust.

The treated tailpipe was developed by analysis, laboratory tests, and engine ground tests.

A ground test survey of the aeroacoustic field inside an untreated tailpipe provided basic information for establishing internal design criteria. Noise sources generated by engine instrumentation probes and tailpipe surface holes were revealed during the survey and later observed in the far field polar spectra.

Trade studies were accomplished on candidate suppressor configurations. Each configuration was evaluated on its applicability to a commercial transport. Weight, cost, performance, and acoustical effectiveness were prime considerations. A configuration consisting of an acoustically treated ring and treatment on the inner surface of the tailpipe was selected.

Detail design of the full scale suppressor include selection of liner materials, placement of acoustical treatment, and detail specification of liner construction. Furnace-brazed, stainless steel, perforated sheet liners were selected on the basis of their uniform acoustic properties, availability of materials, and resistance to contamination by exhaust products. Lining placement, liner depth, and acoustical surface open area were established analytically. The selected lining chosen for the annular passage of the suppressor was tested in the flow duct to verify its acoustic performance. The liner performance agreed with theoretical predictions.

A JT3D engine fitted with a two-ring acoustically treated inlet and a full-length treated fan duct was ground tested with and without the tailpipe treatment. Engine performance and far field acoustic data were obtained.

Analysis of the engine performance data indicated a thrust loss resulting from the treatment of less than 0.5 percent.

The treated tailpipe reduced the peak 5470 Hz fourth stage turbine tone SPL at the design landing approach power setting by 16 dB to 20 dB. The peak second and third stage turbine tones near 7800 Hz were reduced by 10 dB. The turbine tones were suppressed below the level of the jet exhaust for most polar angles.

The acoustic benefit of the treated tailpipe was estimated for landing approach when installed on a 707-320B airplane equipped with the acoustically treated nacelles developed under NASA

contract NAS 1-7129. A reduction of 1.7 PNdB in peak tone corrected perceived noise level (PNLT) was estimated which provided an effective perceived noise level (EPNL) reduction of 0.6 EPNdB after the appropriate duration correction was applied.

A retrofit of 400 707-320B airplanes with treated tailpipes was estimated to increase airplane direct operating costs by less than 0.37 and 0.57 percent for the 1000 nautical mile domestic and the 2500 nautical mile international routes, respectively.

Significant results of the program are:

- Engine exhaust instrumentation was identified to contribute to the far field acoustic spectra of the JT3D engine.
- An analytical technique was successfully applied to the design of acoustic treatment for the high temperature, pressure, and turbine frequency regime of the JT3D tailpipe. Generally, good agreement exists between analytical predictions and test results.
- The manufacture of acoustic panels for the tailpipe environment with a high degree of acoustic property uniformity was demonstrated.

INTRODUCTION

A previous NASA sponsored study and development contract (refs. 1 through 7) was conducted to reduce the compressor noise radiated from a JT3D turbofan engine. A landing approach noise reduction of 15.5 EPNdB was demonstrated by application of acoustic treatment to the inlets and the fan discharge ducts of the nacelle for the 707-320B airplane as shown in figure 1. This significant reduction in fan-compressor noise demonstrated that the unsuppressed turbine generated noise, previously masked by the fan noise, was identified in the spectrum as shown in figure 2.

Consequently, a study was conducted to determine the net contribution of turbine noise to the total perceived noise level (PNL). The results from the study indicated that a noise floor was indeed generated by the turbine and that further reductions in aft radiated noise could not be practically attained without attenuating the turbine noise.

The primary objective of this program, under contract NAS 1-9622, was to demonstrate the capability of applying acoustic treatment in the tailpipe and designing for a given turbine tone frequency and attenuation. This task was to be accomplished with minimum degradation in engine performance and minimum increase in weight and cost. Although large reductions in landing approach noise cannot be achieved by turbine noise suppression of the 707-320B airplanes, the application and extension of lining technology to the high temperature, pressure, velocity, and frequency regime was demonstrated.

The activities and accomplishments of this program are reported in the general sequence in which they occurred. The initial activities in the program were the suppressor design studies which included an internal aeroacoustic survey of the tailpipe, a configuration trade study, and a

suppressor development. Full scale tests were then accomplished to determine the performance of the developed suppressor. The final activity was an economic study to determine the significance of tailpipe acoustic treatment on airplane direct operating costs.

The lining design procedure used in the program is summarized in the appendix.

SYMBOLS

- A Area, square inches
- b Duct height in the y direction, centimeters
- Q_L Centerline
- c Speed of sound relative to the fluid flow in a duct, centimeters per second
- D Hole diameter, inches
- d Backing depth of acoustic panel, centimeters
- dB Decibels referenced to .0002 microbar
- F_g Gross thrust, pounds
- f Sound frequency, Hertz (Hz) or cycles per seconds
- h Duct height in the x direction, centimeters
- i $(-1)^{1/2}$
- k Propagation constant, ω/c , radians/centimeter
- L Face sheet thickness of acoustic panel, inch
- M Mach number, U/c
- N Rotor speed, revolutions per minute
- O.A. (open area) / (total area)
- P Pressure, pounds per square inch absolute
- PNdB Perceived noise, decibels referenced to 0.0002 microbar
- PNL Perceived noise level, PNdB referenced to 0.0002 microbar

p	Acoustic pressure, dynes per square centimeter
SPL	Sound pressure level, decibels referenced to 0.0002 microbar
T	Temperature, $^{\circ}$ R
\bar{T}	Average temperature, weighted on a total enthalpy basis, $^{\circ}$ R
T/R	Thrust reverser
t	Time, seconds
U	Velocity, feet per second; flow velocity in the z direction, centimeters per second
\bar{U}	Average velocity, weighted on an area basis, feet per second
V	Flow velocity in the x direction, centimeters per second
W	Flow velocity in the y direction, centimeters per second
\bar{W}	Acoustic lining impedance, dyne second per cubic centimeter
x	Length in the x direction of a duct, centimeter
y	Length in the y direction of a duct, centimeter
z	Length in the z direction of a duct, centimeter
Δ	Increment
δ	Pressure ratio, P_{am}/P_o
ζ	Acoustic lining impedance normalized by the characteristic impedance of the fluid, ρc .
η	Reduced frequency parameter, $2hf/c$ or hk/π
θ	Temperature ratio, T_{am}/T_o
μ	Real component of $k_x h/\pi$
ξ	Particle displacement, centimeter
ρ	Density of the fluid, grams per cubic centimeter
σ	Real component of k_z/k
τ	Imaginary component of k_z/k

- ϕ Phase angle, degrees
- X Imaginary component of $k_x h/\pi$
- ω Angular frequency, radians per second

Subscripts:

- 0 Sea level standard conditions
- 1 Low pressure compressor rotor
- 2 High pressure compressor rotor
- 4 High pressure compressor discharge station
- 7 Turbine discharge station
- a Annular
- am Ambient conditions
- c Cylindrical
- s Static
- t Total

SUPPRESSOR DESIGN STUDIES

Tailpipe Internal Survey Tests

Full scale internal aeroacoustic survey tests were performed to gain an understanding of the aeroacoustic environment downstream of the turbine and to provide design information for use in a detail design of a suppressor. It was postulated during the previous study (ref. 2) that refraction of the high frequency turbine noise could exist in the presence of large velocity and temperature gradients within the tailpipe. The existence of significant refraction could alter the desired placement of acoustic lining to capture the turbine noise. Radial and axial mapping of the aeroacoustic environment was accomplished to provide the necessary information.

Test installation and instrumentation. – The survey was conducted on a JT3D-3B turbofan engine equipped with a bellmouth inlet, Pratt & Whitney reference fan ducts, thrust reverser adapter and a production 707-320B tailpipe as shown in figure 3. The 707 tailpipe with the thrust reverser adapter (fig. 4) was identical to the tailpipe installation previously flight-tested on the acoustically treated nacelle (ref. 1). The purpose of the adapter extension was to simulate the cross section and length of the production 707 thrust reverser which would be retained for use in a production version of the quiet nacelle.

The internal survey of this baseline tailpipe assembly was accomplished by radially probing the aeroacoustic field at three axial locations. Total and static pressures, total temperature and acoustic spectra were measured at each axial and radial position shown in figure 4. Additional acoustic spectra were obtained from five flush mounted wall microphones located as shown.

Radial probing was accomplished by use of the traversing probe assembly shown in figures 5, 6, and 7. The three instrumentation probes were supported by an airfoil shaped strut to minimize the influence of the probes on the measured aeroacoustic field. The traversing was accomplished by translating the strut into the tailpipe. Two water-cooled bronze blocks were clamped against the strut on opposite sides to provide the necessary cantilever support, a nongalling bearing surface against the strut, and a gas seal for traversing the strut into the tailpipe. The three probes were channeled inside the strut as shown schematically in figure 6. The total and static ports of the pitot-static probe were connected to remote pressure transducers. The total temperature probe was vented at the base of the thermocouple shroud to provide a high temperature recovery factor. Acoustic measurements were obtained by use of the probe tube acquisition system shown in figure 6. This system allowed acoustic pressures to propagate from the probe through the transition block, and to dissipate in the fifty feet of plastic tubing. The constant area passage through the transition block was transformed from a circular entrance to a rectangular cross section at the microphone location and back to a circular area at the block exit to which the tubing was attached. The microphone diaphragm was installed flush with the wall of the rectangular passage. This system allows more uniform acoustic response with frequency than usually obtained with standing wave type probe tubes. The probe tube was water-cooled and capped at its termination to prevent hot gas flow.

The frequency response calibration of the acoustic probe tube system was accomplished by three different methods. The system was first calibrated using a dynamic pressure calibrator which provided dynamic pressures at frequencies from 500 Hz to 16 000 Hz. The response of the system to these dynamic pressures was compared and calibrated to the response of a reference microphone. The second calibration of the system was performed in a free field anechoic chamber to compare the previous calibration to its free field frequency response. The dynamic pressure frequency range was from 50 Hz to 11 000 Hz and the free field response of the system was compared to a standard microphone. The third calibration was conducted in the acoustic flow duct to determine the effect of flow and increased static pressure on the system's response. Both the sensitivity and response of the probe microphone were determined using the flow duct flow conditions. At zero Mach number, the response agreed with the previous two calibrations; however, for a simulated tailpipe Mach number of 0.2, the response calibration had to be corrected upward approximately 2 dB between 1000 Hz to 10 000 Hz.

During the test period, the sensitivity of the acoustic probe tube system was calibrated daily using a piston phone which supplied 124 dB SPL at 250 Hz.

The traversing probe assembly is shown in figure 8(a) mounted to the midstation pad (station 245). The probe traversing mechanism was coupled by a torque tube to a variable drive motor on the ground. The mounting pads for the other two traverse stations and three of the five installed, flush mounted microphones are also shown. Water cooling was supplied to both the traversing mechanism and the wall microphones.

An internal view of the tailpipe with the traversing probe installed is shown in figure 8(b). The probe was canted at a small angle to the tailpipe centerline to compensate for the small angle of

attack produced by the rotation of the exhaust flow. The other two traverse station ports were plugged. The three flush mounted microphones shown were located in the same station planes as the probe was traversed (stations 225, 245, and 258).

Figure 8(b) also shows the engine exhaust gas instrumentation probes just aft of the fourth stage turbine. These probes, six exhaust gas pressure (P_{t7}) and six exhaust gas temperature (T_{t7}) probes, are all cylindrical in shape with the base of the probes having a larger diameter than at the tip.

Results. — The pitot-static pressures and total temperatures measured by the traversing probe were used to calculate the normalized radial velocities shown in figure 9 for each axial station and for five engine speeds. At each axial traverse station the highest velocity occurred in the region near the tailpipe wall. The measurements indicate that extreme velocity gradients develop in the vicinity of the engine tail cone. The average velocity (U) and average total temperature (T_t) were based on the recorded probe data and do not include extrapolations where measurements were not taken.

The total temperature profiles measured by the traversing probe are shown in figure 10. Engine power setting appears to be the most influential factor on radial temperature distribution.

The acoustics measured by the probe microphone and flush mounted microphones were recorded on magnetic tape for each traverse position and engine speed setting run in the test. The acoustic pressures sensed by the probe microphone were continuously recorded as the probe was traversed into the tailpipe. The latter data were used to track the radial SPL variations of the fourth stage turbine tone.

An example of the measured flush mounted microphone spectra is shown in figure 11(a). These spectra were measured by the number two microphone (fig. 4) for an N_1 engine speed of 4300 rpm. The spectra were analyzed by sweeping a 50 Hz narrow bandwidth SPL analyzer from 50 Hz to 10 000 Hz, and recording the SPL as a function of frequency. The discrete tones produced by the fourth, third, and second turbine stages are shown to be above 5000 Hz frequency. The SPL of each tone measured at the tailpipe wall was above 130 dB. The background noise at these frequencies is shown to be more than 20 dB below the level of the turbine tones. Thus, the intensity of the turbine tone noise was considerably greater than the aerodynamic noise in the tailpipe at these frequencies. The first stage turbine tone occurred above 10 000 Hz.

At lower frequencies, the analysis showed that there were two noise peaks (shaded area) appearing above the trend of the background noise centered at 2000 Hz and 3400 Hz, respectively. Additional tests were conducted to determine if the engine exhaust instrumentation probes were causing the noise. The investigation was conducted by process of elimination where the six exhaust gas temperature (T_{t7}) probes were removed first. No significant change occurred in the spectrum for the same engine speed condition. The six exhaust gas pressure (P_{t7}) probes were then removed. Monitoring the engine conditions from the traversing probe, the engine was rerun at the same condition. The resulting spectrum showed an elimination of the shaded portion of the spectrum centered about 2000 Hz in figure 11(a). Thus, the exhaust gas pressure probes contribute to the noise in the spectrum. The noise was produced from von Karman vortices shedding from the probes shown in figure 8(b). The frequency of these sources of noise may be predicted from the ratio of the gas velocity over the probe to the probe diameter (ref. 8). Additional testing in search of the source of the 3400 Hz tone revealed that the noise was generated aerodynamically by the high

velocity exhaust flow over the access holes shown in figure 8(b). The sixteen holes are located near the tailpipe exit plane to provide access to bolts attaching rub strips for the thrust reverser translating sleeve.

An example of the spectra measured by the traversing probe microphone is shown in figure 11(b). The data presented as SPL versus frequency were analyzed by a 50 Hz narrow bandwidth filter. The spectrum shown was measured approximately two inches away from the tailpipe wall. This spectrum, obtained from the acoustic probe, indicates that the probe sensed a greater turbulence component than sensed by a nearby wall microphone (fig. 11(a)). This is evident by the comparative rolloff of the random component of the two spectra with frequency. The noise at lower frequencies was almost 10 dB higher, and the noise generated by the P_{t7} probes was completely masked. However, the 3400 Hz tone emanating from the access holes in the tailpipe appears above the background noise. The turbulence at higher frequencies was not as intense, thus the probe microphone was able to sense satisfactorily the fourth, third, and second stage turbine tones. Note that the SPL levels of the turbine tones measured by the probe and the wall microphones agree quite well.

Since the tailpipe acoustic treatment would be primarily designed to suppress the fourth stage turbine tone, additional 50 Hz narrow band acoustic data of the fourth stage were obtained by tracking the tone for each radial traverse; results are presented in figures 12(a) and 12(b). Radial SPL distributions of the turbine tone are shown in figure 12(a) for five engine speeds. The SPL was found to vary considerably, in a repeatable manner, over the traverse distance into the tailpipe, and the noise level of the tone increased with increase in engine speed. The phenomena responsible for this radial SPL variation cannot be explained in absolute physical terms without more testing; however, these variations could change with alterations in the internal geometry of the tailpipe. Since geometric changes are required in the design of a suppressor, the radial SPL variations do not necessarily represent useful quantitative design information.

The tone level variation for the radial traverses at each station is shown in figure 12(b) for a typical landing approach engine speed. A distorted outline of the tailpipe boundaries is superimposed on the plot to illustrate the axial SPL variations. These results indicate an SPL valley centered about eleven inches from the engine centerline for all three traverse stations. It would be difficult to separate the effects of refraction and modal pressure distribution that contribute to the measured SPL profiles shown in figures 12(a) and 12(b). Therefore, a comprehensive study would be required considering SPL profiles in conjunction with related Mach number profiles to evaluate the measured phenomena.

Suppressor Configuration Trades

Four candidate suppressor configurations were studied in order to choose a reasonable configuration for detail design, fabrication, and full scale test. The four configurations studied are shown in figures 13 and 14. These configurations were chosen for further evaluation because:

- These configurations conformed within the envelope of the NASA quiet nacelle (fig. 11),
- The gas flow path and clam shell door travel (fig. 14) of the production 707 thrust reverser are unaffected by the addition of acoustic treatment in the tailpipe, and

- The suppressor designs do not require engine modifications.

Each of the configurations shown in figures 13 and 14 were designed with identical area of acoustic treatment on the inside surface of the tailpipe shell. The primary differences between the four configurations were in the placement of additional treatment within the tailpipe. Each configuration was evaluated on the basis of weight, performance losses due to internal skin friction, relative acoustic performance, and relative cost to produce. The results of the study are shown in table I. The radial vane concept (fig. 13(a)) was ranked the best in weight, performance, and cost. However, to obtain comparable acoustic performance to the second ranked single ring concept (fig. 14), additional vanes would have been required, and consequently would have increased the weight, performance, and cost penalties over that of the single ring concept. Also, the analytical methods available for prediction of acoustic liner attenuation characteristics apply directly to the geometry of the single ring concept, whereas additional development of the prediction technique would have been required for the radial vane configuration. Thus, considering these trades the single ring concept was selected over the other three suppressor designs.

TABLE I. TAILPIPE TRADE STUDY SUMMARY

ACOUSTIC CONCEPT	Δ (WEIGHT) AIRPLANE LBS	$\left(\frac{F_N}{F_N}\right)^*$ T.O. %	$\left(\frac{C_V}{C_V}\right)^*$ CRUISE %	TREATED AREA, FT ²	MOST ATTENUATION RATING FOR APPROACH	LEAST COST RATING
SINGLE RING	+269	- 0.13	- 0.14	21	2	2
RADIAL VANES	+220	- 0.08	- 0.08	16	4	1
TWO RING	+350	- 0.15	- 0.15	24	3	3
RING WITH RADIAL VANES	+490	- 0.21	- 0.22	23	1	4

*Based on skin friction increase only

Suppressor Development

During the development of the acoustically treated nacelle, shown in figure 1, an experimental investigation (ref. 2) was conducted to identify aft quadrant noise sources. The JT3D-3B test engine was equipped with an acoustically treated inlet and an acoustically treated fan discharge duct. The tests identified high frequency noise emanating from the engine turbine stages. Additional tests were conducted with a 90° elbow jet deflector installed over the engine primary exhaust nozzle. The deflector installation served to deflect the discrete frequency turbine noise upward and away from microphones located in the horizontal plane. A comparison of the horizontal plane microphone data, with and without the jet deflector, revealed that the turbine tones emerged at

least 8 dB above the broadband noise at low power settings. Other data obtained from the flight test nacelles during the program, indicated 12 to 14 dB reductions were required at the 110° azimuth angle where peak turbine noise was measured on a 200-foot polar arc (fig. 2).

The development of the full scale suppressor tested under the present program required choice and placement of acoustic linings to achieve the attenuation requirements indicated by the previous program.


Acoustic panel construction. — A review of available liner face sheet materials indicated that from a cost, durability, and fabrication standpoint, perforated sheet would be the best choice. Application of perforated sheet in the high temperature tailpipe environment would require either a brazed or welded structure. Since the liner face sheet chosen would be continually exposed to the products of combustion, it was felt that deterioration of the liner's acoustic properties from contamination would be less likely to occur for a perforated face sheet. Expediency and a desire to maintain uniformity of liner acoustic impedance properties led to the choice of furnace-brazed, stainless steel perforated sheet over honeycomb liner construction.

Minimal hole blockage due to attachment of the perforated face sheet to the honeycomb core was specified. Several specimens were furnace-brazed to insure that the brazing process utilized on the full scale hardware would satisfy this requirement. Minimum hole blockage was achieved. Photographs of a typical specimen are shown in figure 15. Figure 15(a) shows an edge view of the panel with the honeycomb bonded to the face sheet and impervious backing. Figure 15(b) shows that the brazing alloy did not fill the holes. The only significant blockage which existed was the width of the honeycomb ribbon bridging a few of the holes.

Lining placement and geometry. — The environmental data from the aeroacoustic survey tests and the choice of perforated sheet acoustic panels permitted accomplishment of the detail design of the adopted single ring suppressor configuration (fig. 14).

The lining was designed for maximum suppression of the fourth stage turbine tone at a landing approach N_1 engine speed of 4100 rpm. This engine speed is at the lower extreme of landing approach power settings. The 5470 Hz fourth stage tone at 4100 rpm is the most significant contributor to landing approach PNL.

The radial positioning of the circumferential ring and the choice of perforated sheet open area and honeycomb core depth were accomplished mathematically. The placement was based on the expected environment conditions at the panel midstation (station 260). The remainder of the acoustically treated ring was placed along a streamline passing through the chosen midstation location. The near field attenuation for the chosen ring placement and lining was mathematically predicted to be as shown in figure 16. The attenuation for 19 inches of lining length in the annular passage was estimated to be 8 dB. The lining on the inner surface of the tailpipe and the outer surface of the ring were specified to require an open area of 3.93 percent and a core depth of 0.178 inch. The open area and core depth for the lining on the inner surface of the ring were specified as 1.90 percent and 0.103 inch, respectively. A more detailed description of the lining design procedure is contained in the appendix. The results of a sensitivity study on the effects of manufacturing tolerances and contamination effects on acoustic performance are also presented in the appendix.



Lining performance verification tests. — Acoustic flow duct tests were conducted to verify the acoustic performance of the lining selected for the full scale suppressor. The temperature and pressure environment of the tailpipe could not be simulated in the flow duct; therefore, direct verification of lining performance at design conditions could not be obtained. Consequently, the analytical procedure used to design the lining in the tailpipe environment was also used to predict tailpipe lining performance in the flow duct environment. This analysis corrected for temperature and pressure; actual test section Mach numbers, which corresponded to those in the tailpipe, were used in the analysis. Close agreement between predicted and measured data provided verification of tailpipe liner performance.

The annular passage of the test suppressor was investigated in the flow duct. The annular cross section was approximated by a rectangular duct with two opposing walls lined with acoustic panels as shown in figure 17. Two flow duct test section configurations were used during the tests. The constant area test section, shown in figure 17(a), simulated the average duct height in the suppressor annulus. The convergent test section (fig. 17(b)) was used to simulate the convergence of the annulus.

The mean exhaust gas Mach number in the tailpipe was simulated for the design landing approach condition. Tests were also accomplished at Mach numbers above and below the mean.

The primary emphasis of the flow duct investigation was to verify performance of the selected lining; however, variations in backing depth and face sheet open area were also investigated. The test panel lengths were approximately five inches shorter than the lining selected for the actual tailpipe.

The panels were tested with a broadband random spectrum and a simulated turbine spectrum. The random spectrum, approximately 130 dB SPL, was applied to both the constant and convergent area test section configurations. The 130 dB level was selected to provide face sheet particle velocities near those expected in the engine tailpipe. The simulated turbine spectrum was applied to the constant area configuration only. The broadband portion of this spectrum emanated from the flow duct reverberation chambers. The tones simulating turbine noise were produced by a series of vortex generators shown in figure 18. The vortex generators consisted of nine cylindrical rods which were installed upstream of the panels shown in figure 19. These rods were sized (ref. 8) to generate Karman vortex street tones resulting from air passing over the rods. Five equal diameter rods were sized to generate a tone at the frequency of the fourth stage turbine tone. The remaining four equal diameter rods were sized to simulate a single tone near the frequency of the second and third stage turbine tones.

Flush mounted microphones were installed upstream and downstream of the panels to obtain the lining attenuation spectrum. The spectrum was computed from the difference in spectra measured at the respective microphones.

Typical acoustic spectra obtained from the wall microphones during the turbine tone simulation test are shown in figure 20. The simulated turbine tones were well above the broadband noise and near the desired frequencies, but not as discrete as an actual turbine tone. The spectra show that attenuations of 10 dB for the low frequency tone and 7 dB for the higher frequency tone were obtained with the tailpipe lining.

The theoretical prediction of the attenuation spectrum for the tailpipe treatment exposed to the random spectrum in a constant area duct is compared with the measured spectrum in figure 21. The measured and predicted attenuations show good agreement.

Figure 22 shows the measured attenuation spectrum of the tailpipe lining in the convergent duct.

The results of the flow duct tests indicate that the lining chosen for the annular passage should perform approximately as expected, and no changes should be made in the full scale suppressor lining design.

Full scale suppressor. – The completed full scale suppressor, after fabrication, is shown in figure 23. The acoustically treated ring, which was cantilever supported by six radial struts, consisted of a welded assembly of 12 acoustic panels (six panels on the inner surface and six on the outer surface). Thermal expansion provisions were provided at each strut attachment point on the tailpipe shell. Six larger acoustic panels were mounted to tailpipe longerons to provide treatment on the inner surface of the tailpipe.

The perforated sheet panels, fabricated for each surface of the tailpipe, is shown in figure 24 prior to assembly. Each panel was carefully inspected. No significant hole blockage was evident, and their average geometric properties are shown in figure 24. A comparison between the design and final hardware specifications are summarized in table II. The open areas were 2.6 and 12.5 percent below the design specifications. Core depths were slightly above the design specifications. The effect of the deviations on the acoustic performance of the linings are considered negligible. The expected acoustic differences are discussed in the appendix.

TABLE II. PERFORATED SHEET ACOUSTIC LINING DATA

SPECIFICATION ITEM	TAILPIPE WALL LINING		RING OUTER SURFACE LINING		RING INNER SURFACE LINING	
	DESIGN SPECIFICATION	FABRICATED HARDWARE	DESIGN SPECIFICATION	FABRICATED HARDWARE	DESIGN SPECIFICATION	FABRICATED HARDWARE
FACE SHEET OPEN AREA, %	3.93	3.44	3.93	3.44	1.90	1.85
HOLE DIAMETER, INCH	0.039	0.038	0.039	0.038	0.039	0.038
FACE SHEET THICKNESS, INCH	0.032	0.031	0.032	0.031	0.032	0.034
LINING CORE DEPTH, INCH	0.178	0.183	0.178	0.186	0.103	0.105
HONEYCOMB CELL SIZE, INCH	0.375	0.375	0.375	0.375	0.375	0.375

FULL SCALE TESTS

Ground tests were accomplished to determine the acoustic effectiveness of the treated tailpipe and any associated engine performance changes. The test data were used to estimate the reduction in landing approach noise when the tailpipe suppressor is retrofitted with the quiet nacelle (ref. 1) to a 707-320B airplane.

Test Installation and Instrumentation

The far field acoustic test was conducted on the same test stand and engine used for the internal tailpipe survey. For this test, a flightworthy quiet nacelle, developed in reference 1 program, was installed on the engine as shown in figure 25. This nacelle was equipped with an acoustically treated inlet and a long, treated fan duct. The nacelle, with the production 707 primary tailpipe installed, was used as the baseline. After measurement of the baseline noise and performance, the untreated tailpipe was replaced by the treated tailpipe, and the aft radiated exhaust noise was measured.

The thrust was measured by a thrust load cell and associated signal conditioning and read-out equipment. The load cell was located in the engine mounting strut as shown in figure 25. Thrust calibration of the load cell and associated equipment was accomplished by pulling the engine mounted on the stand with a mechanical loading fixture and comparing the measured load with a standard reference load cell.

Far field acoustic data were obtained from a 200-foot polar array of microphones arranged as shown in figure 26. The microphones were oriented to measure the aft radiated noise. At each angle, microphones were placed on the ground plane and at the level of the engine centerline. The ground plane between the engine and the microphones was concrete.

Views of the treated tailpipe after installation are shown in figure 27. The photographs show the fan exhaust area at the outer perimeter, the annular passage exhaust area between the tailpipe wall and the ring, and the cylindrical passage exhaust area inside the ring. The annular passage between the fan nozzle and tailpipe wall provides an ejector pump to aspirate accessory compartment cooling air. This area was substantially blocked by a flange which was incorporated on the aft portion of the treated tailpipe to allow removal of the tailpipe nozzle for mismatch trimming of the exhaust area, if required. A more detailed view of the blocked ventilation passage is shown in detail B of figure 14.

Results

The engine was run at five low power settings in the landing approach thrust range to obtain detailed acoustic performance data for both the treated and untreated tailpipes. Acoustic and performance data were also taken at higher power settings.

The measured thrust performance of the nacelle with a production 707-320B tailpipe (baseline) and the treated tailpipe is shown in figure 28. The measured thrust loss was 4.9% which was considerably more than the estimated losses based on skin friction calculations (table I). An

analysis of the detailed engine matching parameters measured during the test ($N_1/\sqrt{\theta_{amb}}$, $N_2/\sqrt{\theta_{amb}}$, P_{t7}/P_{amb} , and P_{s4}/P_{t7}) indicated that 1.7% of the loss could be recovered by a simple adjustment of nozzle exit area. Additional calculations revealed that restriction of the accessory cooling duct, due to the flange (detail B, fig. 14) on the treated tailpipe, could cause at least 2.7 percent thrust loss. Since both losses could be easily eliminated in a production program, a maximum of 10% of the measured thrust loss can be attributed to the tailpipe treatment.

Based upon the above analysis of the engine performance measurements, it is estimated that the performance penalty due to the treated tailpipe is less than 0.5 percent.

Visual inspection of the acoustic treatment was conducted after the full scale tests. No contamination was observed on the treatment that would affect the acoustic properties. A thin film of carbon residue was on the surface but was easily wiped off. The scrubbing action of the exhaust gas would prevent any buildup of the carbon. No apparent deterioration in acoustic panel structural characteristics was evident as a result of the tests. Operational problems, such as fuel collection in the panel sandwich structure, did not occur during the testing.

Far field acoustic measurements were recorded at each engine N_1 speed. Examples of the measured far field noise spectra for both the baseline and treated tailpipe are shown in figure 29 for the ground microphone located 120° from the inlet centerline. These particular spectra represent a 50 Hz narrow bandwidth analysis of the aft exhaust noise at the design engine speed ($N_1 = 4100$ rpm). These spectra were not corrected for the pressure doubling which results from the proximity of the microphone to the ground plane. Comparison of the jet noise from 50 Hz to 1000 Hz for the two tailpipes indicate that the thrust loss with the treated tailpipe did not affect the jet noise significantly.

At higher frequencies, the jet noise gradually reduced to a lower SPL. The first stage fan tone was measured at 2400 Hz. For the baseline, the fourth and third stage turbine tones had an SPL of 87 dB and 80 dB, respectively. With the treated tailpipe, the turbine tones were suppressed to about 71 dB. Note the noise floor, which was previously assumed to be jet noise in the frequency regime of the turbine tones, was reduced 4 or 5 decibels.

The second stage turbine tone was highly directional and did not appear above the background noise for this polar angle.

Note that the noise generated by the engine exhaust instrumentation probes, detected previously during the internal survey, was observed in the far field spectra shown in figure 29. The tone generated by the access holes in the baseline tailpipe was also observed in the spectrum shown in figure 29(a). These holes were not included in the development of the treated tailpipe and, thus, the associated tone was nonexistent in figure 29(b).

Figure 30 shows the same polar angle spectra, except these spectra were measured by the engine centerline level microphone. The magnitude of the turbine tone SPL measurements are shown to be similar to the ground microphone measurements. However, the jet noise spectra indicates an SPL dip centered at about 1800 Hz. This dip was caused by destructive interference from the interaction of a reflected sound wave, from the ground plane, with a nonreflected wave. These cancellations, however, do not significantly affect the suppression difference calculation between the baseline and the treated tailpipe since this effect occurs in both spectra.

A 50 Hz narrow bandwidth time history analysis was conducted on each turbine tone at each polar angle to determine tone directionality and the amount of suppression attained by the treated tailpipe. The time duration for each history was 40 seconds. Examples of the time history results are shown in figures 31, 32, and 33.

Figure 31 is a comparison of the acoustics measured by the ground and engine centerline level microphones for the fourth stage turbine tone at an engine N_1 speed of 3900 rpm. The polar angle direction of tone propagation was primarily from 100 to 120 degrees from the inlet centerline. Suppression of the turbine tone varied from 10 to 19 decibels. The two microphones measured similar polar signatures.

Figure 32 shows the suppression performance of the treated tailpipe on the fourth and second stage turbine tones for the design N_1 speed of 4100 rpm. Suppression of fourth stage tone, measured by the ground microphone, was 16 dB and 20 dB at the 110° and 120° polar angles; second stage tone was suppressed about 10 dB at the 110° polar angle. The propagation direction for each turbine tone was about the same; however, the second and third stage turbine tones had more narrow polar signatures.

The suppression performance of the treated tailpipe on the fourth stage turbine tone at two additional approach power settings is shown in figure 33. The curves show at least 10 dB suppression at the peak polar angle for both off-design engine conditions.

A comparison of the peak attenuation of the fourth stage turbine tone at power settings between 3900 and 4600 rpm indicates that the treatment was performing best at the design speed of 4100 rpm.

One-third octave bandwidth analysis was also conducted on the noise measured by each microphone. Figure 34 is an example of this analysis for the ground microphone acoustics at 110 degrees from the inlet centerline; N_1 engine speed was 4100 rpm. The shaded area represents the attenuation accomplished by the treated tailpipe. Approximately 11 dB suppression was obtained near the frequency of the fourth stage turbine tone (5470 Hz). The second and third stage turbine tones were attenuated approximately 7 dB at this angle; reduction in perceived noise for this condition was 3.9 PNdB.

To determine the effective perceived noise level (EPNL) reduction accomplished by the treated tailpipe during landing approach, a flyover time history of the perceived noise reduction was estimated from the 200 foot polar array microphone data. These PNL data were then superimposed in figure 35 on the flyover data previously measured during the reference 1 program on the same nacelles without the treated tailpipe. The figure shows PNL versus relative time flying over a ground microphone for the baseline 707-320B airplane and for the same airplane with the NASA quiet nacelle installed. An EPNL reduction of 15.5 EPNdB was estimated for the quiet nacelle for the flight and engine conditions specified in figure 35. The dotted line represents the PNL reduction accomplished by the treated tailpipe with the maximum PNL reduction of 1.7 PNdB at a relative time of approximately one second. After application of the appropriate duration correction, a reduction in EPNL of 0.6 EPNdB can be attributed to the treated tailpipe.

ECONOMIC STUDIES

A study on the economics of retrofitting treated tailpipes on a Boeing 707-320B was accomplished to determine their effect on direct operating costs (DOC) of the airplane. The study assumes that the treated tailpipes would be installed at the time the NASA quiet nacelles would be retrofitted on the airplane. Therefore, the procedures and ground rules used in the previous economic study, for NASA contract NAS 1-7129 (ref. 6), were adopted to estimate the DOC changes.

In estimating the tailpipe retrofit costs, items such as fabrication techniques, date of go-ahead, number of kits produced, production rate, and the method of performing the installation in airline service were specified. The production schedule was the same as described in reference 6. This schedule provides a production rate of 16 airplane sets per month with a total production of 500 shipsets (2000 kits). Twenty percent of the total production were spares. Full production would start 27 months after go-ahead. It was assumed that the installation of the treated tailpipe would occur at the same time the quiet nacelles were installed. No installation charge was considered for retrofitting the tailpipe. Based on these assumptions, the estimate for the price of retrofitting the tailpipe is shown in figure 36(a). The cost per shipset is shown to approach \$33 100 after a total production of 500 shipsets. The add-on costs to the quiet nacelle retrofit is shown as the shaded area in figure 36(b).

The DOC increases attributed to the treated tailpipe retrofit were estimated for both the 1000 nautical mile domestic route and the 2500 nautical mile international route using the standard ATA flight profile rules. The same flight operation items listed in reference 6 were implemented in the estimate. As shown in table III, the depreciation period assumed was 12 years for the airplane and five years for both the quiet nacelle and the treated tailpipe; airplane utilization was fixed at 3800 hours. The factors affecting the DOC increases were tailpipe costs, including spares, weight increase, and thrust penalty.

TABLE III. DOC INCREASE OVER FLIGHT-WORTHY QUIET NACELLE

<u>Airplane data</u>	<u>Treated tailpipe data</u>		
Model:	707-320B	Cost/Shipset:	\$40,000
Utilization:	3800 hr	ΔWeight/Shipset:	+ 269 lb
Flight profile:	Standard ATA	Thrust penalty:	0.5%
Depreciation:	12 yr	Depreciation:	5 yr

	1000 n. mi. Domestic route	2500 n. mi. International route
Quiet nacelle DOC cents per seat st. mi.	1.350	1.220
DOC with treated tailpipe, cents per seat st. mi.	1.355	1.227
Percentage breakdown of increase:		
Crew pay	0	0
Fuel and oil	29.1	38.4
Insurance	5.5	4.7
Maintenance	0	0
Depreciation	<u>65.4</u>	<u>56.9</u>
TOTAL	100.0%	100.0%

Table III shows the treated tailpipe's estimated DOC increase over the flightworthy quiet nacelle. For the domestic and international routes, the DOC increases were 0.005 and 0.007 cents per seat per statute mile, respectively. The itemized breakdown of the DOC increase is also shown in table III. Crew pay increase and maintenance of the tailpipe was considered negligible in the estimate. Depreciation was the largest contributor to the DOC increase.

CONCLUDING REMARKS

The application of analytical acoustic liner design procedures was successfully applied to suppress the high frequency turbine noise in the high temperature, pressure, and velocity environment of the JT3D engine tailpipe. It was also demonstrated that acoustic panels for this extreme environmental application can be fabricated with a high degree of final product acoustic uniformity. This technology application, although not demonstrating a large EPNL reduction for the 707-320B airplane, may be applied to future applications.

The JT3D engine exhaust instrumentation probes and surface holes in the production 707 tailpipe were shown to contribute to the far field spectra as evidenced from this program. In the future, as engines become quieter, careful attention must be given to the detail design of engine instrumentation probes and internal duct surfaces to prevent aerodynamic noise generation and to ensure a quiet installation.

The ground plane microphones used during the far field measurements appeared to produce superior spectral detail when compared to the engine centerline microphone data. This may only be true for the low wind case in the absence of extreme surface temperature gradients. Further research should be conducted to ascertain the influence of surface winds and temperature gradients on ground microphone data.

The Boeing Company

Wichita Division

Wichita, Kansas, May 31, 1971



APPENDIX

ACOUSTIC LINING DESIGN ANALYSIS PROCEDURE

Available analytical methods were used in this study to determine the optimum tailpipe acoustic treatment for suppressing the turbine tones. The procedure for applying these methods is outlined in figure 37. The analysis was basically a boundary value problem for the transmission and attenuation of sound in an acoustically treated duct. The mathematical model used in the acoustic lining optimization is based on a semi-infinite duct which is derived for either rectangular or cylindrical ducts. To exemplify the procedure, the following mathematical model is derived with the rectangular coordinate system shown in figure 38.

The airflow in the duct is inviscid, nonturbulent and has a uniform velocity U along the z axis of the duct. The acoustic impedance of the unlined duct walls is assumed infinite while the acoustically treated wall at $x = h$ has an impedance which is normally reacting. This assumes that the impedance of the acoustic lining is independent of the angle of incidence of the acoustic wave; hence, the acoustic characteristics of the lining are completely specified. The plane wave acoustic source is phased at $z = 0$ and the propagation of these waves down the duct are evaluated as a function of Mach number, frequency, duct geometry, and lining impedance.

The acoustic wave equation for the duct environmental conditions described above is given by,

$$c^2 \nabla^2 p = \left(\frac{\partial}{\partial t} + U \frac{\partial}{\partial z} \right)^2 p \quad (1)$$

where

c = the speed of sound relative to the fluid flow in the duct

p = the acoustic pressure

U = the uniform duct flow velocity.

The convected wave equation (1) can be solved by separation of variables and by assuming the following solution for simple harmonic theory:

$$p = XYZT \quad (2)$$

where $X = C_x \cos k_x x + S_x \sin k_x x \quad (3)$

$Y = C_y \cos k_y y + S_y \sin k_y y \quad (4)$

$Z = e^{-ik_z z} \quad (5)$

$T = e^{i\omega t} \quad (6)$

APPENDIX

$C_x, S_x, C_y,$ and S_y are constants which are determined by the boundary condition at the duct walls. $k_x, k_y,$ and k_z are propagation constants in the respective coordinate direction.

The k_z propagation constant down the duct established the attenuation properties of the acoustically treated duct in terms of wall impedance. An expression for k_z is determined by substitution of the assigned solution into the wave equation (ref. 9).

Thus,

$$k_z = \frac{-Mk + \left[k^2 - (1-M^2)(k_x^2 + k_y^2) \right]^{1/2}}{(1-M^2)} \quad (7)$$

where

$$M = U/c$$

$$k = \omega/c .$$

Since k_x and k_y are functions of the boundary condition, the continuity of particle displacement at the duct walls is assumed. The equation of motion for fluid flow normal to the walls is given by:

$$\rho \frac{D^2 \xi_1}{Dt^2} = \frac{\partial p}{\partial x} \quad (8)$$

where ξ_1 = the particle displacement normal to the wall at $x = h$

ρ = the density of the fluid

$\frac{D}{Dt}$ = the substantial derivative which is equivalent to

$$\left(\frac{\partial}{\partial t} + U \frac{\partial}{\partial z} + V \frac{\partial}{\partial x} + W \frac{\partial}{\partial y} \right).$$

Since there is no velocity component in the x and y directions, equation (8) can be reduced to

$$\rho \left(\frac{\partial}{\partial t} + U \frac{\partial}{\partial x} \right)^2 \xi_1 = - \frac{\partial p}{\partial x} . \quad (9)$$

The relationship between pressure and particle velocity at the lined wall, $x = h$, is

$$\rho c \zeta = \frac{p}{\frac{\partial \xi_2}{\partial t}} \quad (10)$$

where ζ = the acoustic lining impedance normalized by the characteristic acoustic impedance of the fluid, ρc

ξ_2 = the particle displacement in the lining material.

The boundary condition at the lined wall surface has the particle displacement equivalence of ξ_1 and ξ_2 . If harmonic motion is assumed,

$$\frac{\partial \xi}{\partial t} = i\omega \xi. \quad (11)$$

APPENDIX

Hence,

$$\xi = \frac{p}{i \omega \rho c \zeta}. \quad (12)$$

Making use of the assumed solution of equation (5), it follows that

$$\frac{\partial}{\partial z} = -i k_z. \quad (13)$$

The equation of motion (9) can now be written as

$$\rho (i\omega - iUk_z)^2 \frac{p}{i \omega \rho c \zeta} = -\frac{\partial p}{\partial x} \quad (14a)$$

or

$$\frac{i}{k\zeta} (k - Mk_z)^2 p = -\frac{\partial p}{\partial x}. \quad (14b)$$

Since all walls have an infinite impedance except at $x = h$ and substituting the assumed solution into (14b), the following results:

$$-\frac{i}{k\zeta} (k - Mk_z)^2 = k_x \tan(hk_x) \quad (15a)$$

and expanding fully,

$$\frac{i}{k\zeta} \left(k - \frac{M \left\{ -Mk + \left[k^2 - (1 - M^2) (k_x^2 + k_y^2) \right]^{1/2} \right\}}{1 - M^2} \right)^2 = k_x \tan(hk_x). \quad (15b)$$

Making use of the fact that the walls normal to y have an infinite impedance then, from the boundary conditions,

$$k_{ym} = \frac{m\pi}{b} \quad (16)$$

where b is the duct height in the y direction.

Incorporation of (16) into (15b) and simplifying gives

$$\frac{i}{(1 - M^2)^2 k \zeta} \left(k - M \left\{ k^2 - (1 - M^2) \left[k_{xn}^2 + \left(\frac{m\pi}{b} \right)^2 \right] \right\}^{1/2} \right)^2 = k_{xn} \tan(hk_{xn}) \quad (17)$$

where m and n are the mode numbers associated with the y and x directions.

By introducing $\eta = \frac{2hf}{c} = \frac{hk}{\pi}$, equation (17) becomes

$$\frac{i\pi\eta}{(1 - M^2)^2 \zeta} \left(1 - M \left\{ 1 - (1 - M^2) \left[\left(\frac{hk_{xn}}{\pi\eta} \right)^2 + \left(\frac{mh}{\eta b} \right)^2 \right] \right\}^{1/2} \right)^2 = hk_{xn} \tan(hk_{xn}), \quad (18)$$

APPENDIX

k_{xn} is a complex quantity which can be represented as

$$k_{xn} = \frac{\pi}{h} (\mu_n + i X_n). \quad (19)$$

Substituting this relation, equation (18) becomes

$$\frac{i \pi \eta}{(1 - M^2)^2 \xi} \left(1 - M \left\{ 1 - (1 - M^2) \left[\left(\frac{\mu_n + i X_n}{\eta} \right)^2 + \left(\frac{mh}{\eta b} \right)^2 \right] \right\}^{1/2} \right)^2 = \pi (\mu_n + i X_n) \tan \left[\pi (\mu_n + i X_n) \right]. \quad (20)$$

After clearing the imaginary component from (20), the normalized wall impedance down the acoustically treated duct may be expressed as:

$$\frac{\bar{W}}{\rho c \eta} = \frac{\left(1 - M \left\{ 1 - (1 - M^2) \left[\left(\frac{\mu_n + i X_n}{\eta} \right)^2 + \left(\frac{mh}{\eta b} \right)^2 \right] \right\}^{1/2} \right)^2 \coth \left[-i \pi (\mu_n + i X_n) \right]}{(1 - M^2)^2 (\mu_n + i X_n)} \quad (21)$$

where \bar{W} is the acoustic lining impedance, $\rho c \xi$.

For zero Mach number, equation (21) agrees exactly with Cremer's work (ref. 10).

The development of the least attenuated acoustic mode optimization program requires an extension to the previously developed theory to establish an attenuation constant for the individual acoustic modes that are propagated down the acoustically treated duct. The attenuation constants are a function of Mach number, frequency, duct geometry, and lining impedance \bar{W} .

From the earlier assumed solutions,

$$Z = e^{-ik_z z} \quad (5)$$

the acoustic pressure, p , down the duct is assumed to be a function of z .

The attenuation down a duct is a function of pressure at a given station relative to that at a reference station. The attenuation in decibels per centimeter of lining is given by,

$$\frac{dB}{cm} = 20 \log_{10} \left| \frac{P(z = z_0 + 1)}{P(z = z_0)} \right|. \quad (22)$$

APPENDIX

The pressure in the duct is a function of the propagation constant, k_z , as well as other factors and is, in general, a complex number which can be expressed as,

$$k_z = k (\tau - i\sigma). \quad (23)$$

The attenuation equation (23) may now be expressed as

$$\frac{dB}{cm} = 20 \log_{10} e^{k\sigma} = 8.68 k\sigma \quad (24a)$$

or using the fact that $\eta = 2hf/c$, then

$$\frac{dB}{cm} = 27.3 \frac{\sigma\eta}{h}. \quad (24b)$$

Since $\sigma\eta$ is the reactive part of the propagation constant, k_z , down the duct, the following expression is considered,

$$k_z = \frac{-Mk + \left[k^2 - (1 - M^2) k_x^2 \right]^{1/2}}{1 - M^2}. \quad (7)$$

Substituting (23) and

$$k_x = \frac{\pi}{h} (\mu + iX) \quad (25)$$

into (7), the following results:

$$\eta (\tau - i\sigma) = \frac{-M\eta + \left[\eta^2 - (1 - M^2) (\mu + iX)^2 \right]^{1/2}}{1 - M^2}. \quad (26)$$

Solving for $\sigma\eta$

$$\sigma\eta = \frac{1}{(1 - M^2)^{1/2}} \left(\frac{1}{2} \left\{ \left[\left(\frac{\eta^2}{1 - M^2} - \mu^2 + X^2 \right)^2 + (2\mu X)^2 \right]^{1/2} - \left(\frac{\eta^2}{1 - M^2} - \mu^2 + X^2 \right) \right\} \right)^{1/2}. \quad (27)$$

At this point, the attenuation constant, $\sigma\eta$, is established for the least attenuated mode that provides the greatest attenuation per unit lining length. This can be accomplished by using (27). A set of design conditions is selected, as shown in block 1 of figure 37, which includes duct geometry, frequency of optimization, lining material type, and Mach number. These factors are used along with μ and X estimates to calculate a $\sigma\eta$. Next, holding $\sigma\eta$ constant a set of μ and X variables can be generated for the first Riemann sheet by incrementing either μ or X and solving for the remaining variable. This procedure is repeated until μ and X variables force $\sigma\eta$ through a branch cut (fig. 39). At this time, the original $\sigma\eta$ is increased by an increment and a new set of μ and X variables are generated as before.

APPENDIX

The lines of constant $\sigma\eta$ are plotted on a graph (fig. 39) of normalized admittance $\frac{\rho c \eta}{\bar{W}}$ versus phase angle ϕ .

The admittance may be determined since μ, χ , duct geometry and Mach number are known for the frequency being investigated. These variables are also used to calculate the corresponding phase angle using the following equations:

$$\phi = \tan^{-1} \left[\frac{(1 - M^2) (2 \mu \chi)}{\eta^2 - (1 - M^2) (\mu^2 - \chi^2)} \right]. \quad (28)$$

As the lines of constant $\sigma\eta$ increase, the enclosed areas will converge to a point as shown in figure 39. This point corresponds to the maximum attenuation constant that can be obtained for the least attenuated acoustic mode. Since the values of μ and χ are also known, the lining impedance, \bar{W} , can be determined.

The above mathematical model and procedure was incorporated into a digital computer program to compute the lining impedance required to give maximum attenuation for the least attenuated acoustic pressure mode. Another digital program was used to compute the lining impedance for a cylindrical duct configuration. These two programs comprised the acoustic lining optimization program, as shown in block 2 of figure 37, to determine the optimum lining impedance in both the annular and cylindrical flow passages of the single ring tailpipe configuration. For suppression of the turbine tones, the fourth stage turbine tone frequency of approximately 5500 Hz was selected as the optimization frequency.

To establish the lining geometry, the impedance of the acoustic lining must match the impedance determined by the optimization program. This objective was accomplished by using the following semiempirical impedance model (block 3, fig. 37):

$$\begin{aligned} \frac{\bar{W}}{\rho c} = & \frac{1}{\text{O.A.}} \left(\frac{0.0762 (T_{s7}/519)^2 L}{(P_{s7}/14.7) [(T_{s7}/519) + 0.416]} \right. \\ & + \frac{3.74 \times 10^{-5} (T_{s7}/519)^{0.75} \sqrt{f}}{\sqrt{(P_{s7}/14.7) [(T_{s7}/519) + 0.416]}} \left[\frac{L}{D} + (1 - \text{O.A.}) \right] + 0.1085 M \\ & + i \left\{ \frac{4.69 \times 10^{-4} f}{\sqrt{T_{s7}/519}} \left[L + 0.85 D \left(1 - 0.7 \sqrt{\text{O.A.}} \right) e^{-(8.65 M^2 + 0.8192M)} \right] \right. \\ & \left. - (\text{O.A.}) \cot \left(\frac{2\pi f d}{c} \right) \right\}. \quad (29) \end{aligned}$$

For a specified face sheet thickness, L , and hole diameter, D , the impedance model predicted the required face sheet open area, O.A. , and core backing depth, d .

APPENDIX

The internal survey tests showed that only moderate SPL's exist within the tailpipe at the design power setting. Consequently, the impedance of the liner was considered independent of SPL at the design condition. This conclusion can be deduced from the measurements of Feder and Dean (ref. 11). The form of the model and the empirical constants were established in previous unpublished Boeing studies. A similar impedance model has been presented in reference 12.

Initially, both the rectangular and cylindrical duct optimization programs were used in block 5, figure 37, to analyze a section of the lined passages, at midspan station 260 (fig. 4), which established preliminary lining impedance and attenuation rate (dB/cm) for an assumed duct height or diameter.

The above procedure was then repeated for various duct heights or radial positions of the ring at station 260 to establish attenuation differences between the annular flow passage and the cylindrical flow passage. The purpose of this repetitive procedure was to determine the optimum ring location (block 4, fig. 37) which would give equal acoustical power transmission between the two flow passages. The relation used for estimating equal acoustical power was simply a logarithmic ratio of the passage areas at the termination point of the lining:

$$(\text{Attenuation}) = 10 \log (A_{\text{Annulus}}/A_{\text{Cylinder}}).$$

The above expression and the computer attenuation differences determined from the optimization program were compared as shown in figure 40. The area ratio at the crossover point ($A_A / A_C = 3.51$) was used as the optimum ring location at the lining midspan (station 260).

The circumferential treated ring was then oriented to have zero angle of attack to the flow streamlines which were determined from a potential flow analysis of the airflow in the tailpipe. With angle of attack and midspan position set for the ring, the resulting area ratio at the termination point of the lining was 3.89. Since the equal power radiation constraint is based on the cross sectional area at the end of the lining, the design attenuation difference requirement was then reestablished as 5.9 dB, as shown in figure 40.

A multimode analysis (block 7, fig. 37) was then conducted by digital computing to determine more closely the attenuation difference within the convergent flow passages. This analysis considers the propagation effects of the higher acoustic modes on the attenuation properties of the acoustically lined ducts.

The multimode analysis procedure consists of a set of digital computing programs that can evaluate the acoustic performance of an acoustic lining over a frequency spectrum for ducts having rectangular or circular duct geometries. These programs utilize as inputs either a complex lining impedance or a lining geometry, the acoustic environmental condition, and the geometric constraints of the duct to compute the acoustic performance of the lining.

As shown in equation (21), the attenuation of each mode is proportional to $\sigma\eta$. Thus, the individual modal attenuations were calculated for a wall impedance corresponding to the maximum $\sigma\eta$ for the least attenuated mode, which was determined previously in the acoustic lining optimization program (block 2). The modes that did exist were assumed to have equal pressure amplitude at the beginning of the lining. These modal attenuations were multiplied by the incremental length of the lining and subtracted from the modal amplitude distribution to establish

APPENDIX

the attenuated distribution. This distribution was then summed to give the attenuated sound pressure level for the center frequency of 5470 Hz.

Since the duct environmental factors (Mach number, SPL, geometry, etc.) varied down each duct, the attenuation characteristics of the total lining were determined in incremental steps. This was accomplished by breaking the lining up into small increments of length and computing the respective attenuations of the various acoustic modes that could propagate in the ducts. The individual modal attenuations at each frequency were combined into a total attenuation over the increment of lining being evaluated. At this time, variables such as SPL, duct geometry variation, Mach number, thermodynamics, etc., were adjusted for the next increment of lining length so that an additional increment of attenuation could be computed. This procedure was repeated throughout the entire length of lining for each duct passage so that a realistic estimate of attenuation with respect to frequency could be established.

The results of this analysis are presented in figure 16. The peak attenuations, determined for the 5470 Hz design frequency, were 14 dB and 7.9 dB, respectively, for the annular and cylindrical passages. The attenuation difference was 6.1 dB which indicates, as shown in figure 40, that the predicted lining configuration closely meets the design goals for equal power radiation at the duct termination.

A parametric study (block 8) was then conducted to determine the effects of hole blockage and core depth variations on the lining performance. These effects were determined by inputting various lining open areas and core depths into the impedance mathematical model and the multimode analysis program and computing the peak attenuation and tuning frequency for each variation. These inputs and results were then compared (block 9) to the design lining geometry and attenuation presented in figures 41 through 44.

Figures 41 and 42 show the effect of face sheet open area changes caused by either hole blockage contamination or variation in face sheet tolerances. Figures 43 and 44 depict the effect of core depth deviation caused primarily by the fabrication process and tolerance variation of the core thickness. The deviation in lining attenuation from optimum at the design tuning frequency is shown in figures 41 and 43. The change in peak attenuation from the optimum design attenuation is presented in figures 42 and 44. In addition, figures 42 and 44 show the peak attenuation frequency shift from the design frequency.

As shown in table II, the test hardware geometry varied from the design specifications and could have severely affected the lining acoustic performance unless close control of the manufacturing technique was applied. The parametric studies showed that the geometry deviations were within acceptable tolerances as presented by the dashed lines in figures 41 through 44. The dashed lines exemplify the performance changes in the annular passage caused by the open area and core depth deviations from the design specifications. Experimental near field data were not obtained to fully substantiate these performance changes. However, far field data did indicate that the overall attenuation objectives were met and the lining obtained best performance at the design power setting of 4100 rpm.

REFERENCES

1. The Boeing Company: Study and Development of Turbofan Nacelle Modifications to Minimize Fan-Compressor Noise Radiation. Program Summary. NASA CR-1711, 1970.
2. The Boeing Company: Study and Development of Turbofan Nacelle Modifications to Minimize Fan-Compressor Noise Radiation. Acoustic Lining Development. NASA CR-1712, 1970.
3. The Boeing Company: Study and Development of Turbofan Nacelle Modifications to Minimize Fan-Compressor Noise Radiation. Concept Studies and Ground Tests. NASA CR-1713, 1970.
4. The Boeing Company: Study and Development of Turbofan Nacelle Modifications to Minimize Fan-Compressor Noise Radiation. Flightworthy Nacelle Development. NASA CR-1714, 1970.
5. The Boeing Company: Study and Development of Turbofan Nacelle Modifications to Minimize Fan-Compressor Noise Radiation. Sonic Inlet Development. NASA CR-1715, 1970.
6. The Boeing Company: Study and Development of Turbofan Nacelle Modifications to Minimize Fan-Compressor Noise Radiation. Economic Studies. NASA CR-1716, 1970.
7. The Boeing Company: Study and Development of Turbofan Nacelle Modifications to Minimize Fan-Compressor Noise Radiation. Subjective Evaluation Tests. NASA CR-1717, 1970.
8. Schlichting, Hermann: Boundary Layer Theory. Fourth ed., McGraw-Hill Book Co., Inc., 1960.
9. Eversman, Walter: The Effect of Mach Number on the Tuning of an Acoustic Lining in a Flow Duct. J. Acoust. Soc. Am., Vol. 48, No. 2, 1970, pp. 425 - 428.
10. Cremer, L.: Theorie der Luftschall-Dämpfung in Rechteckkanal mit Schluckender Wand and das sich Dabei Ergebende Hochste Dämpfungmass. Acustica, Vol. 3, 1953, pp. 249 - 263.
11. Feder, Ernest; and Dean, L. D., III: Analytical and Experimental Studies for Predicting Noise Attenuation in Acoustically Treated Ducts for Turbofan Engines. NASA CR-1373, 1969.
12. Rice, Edward J.; Feiler, Charles E.; and Acker, Loren W.: Acoustic and Aerodynamic Performance of a 6 Foot Diameter Fan for Turbofan Engines. Supplement III, Performance with Noise Suppressors. NASA TN D-6178, 1971.

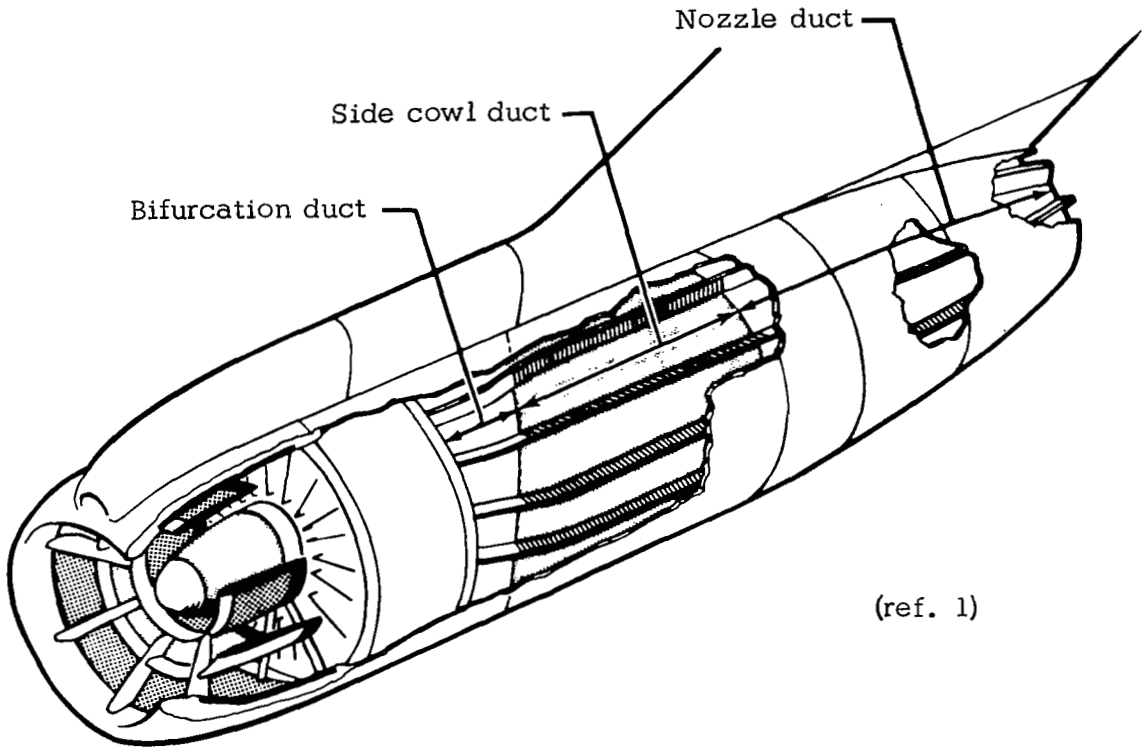


Figure 1. NASA quiet nacelle

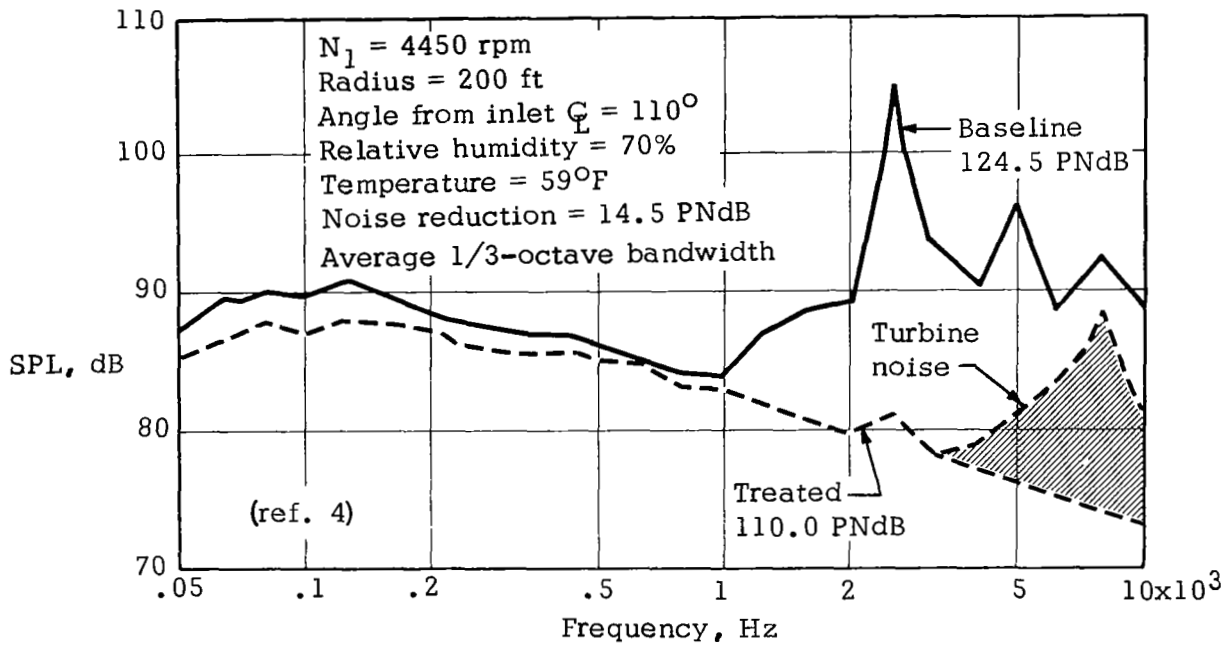


Figure 2 . Maximum fan exhaust noise at approach power, ground test

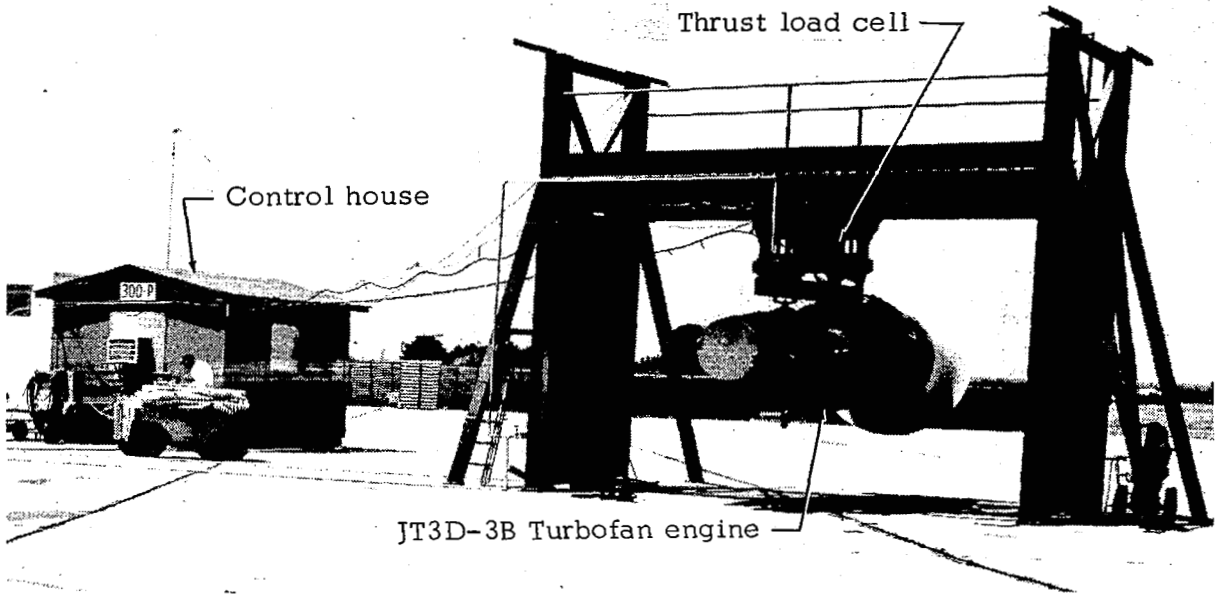


Figure 3 . Engine test installation

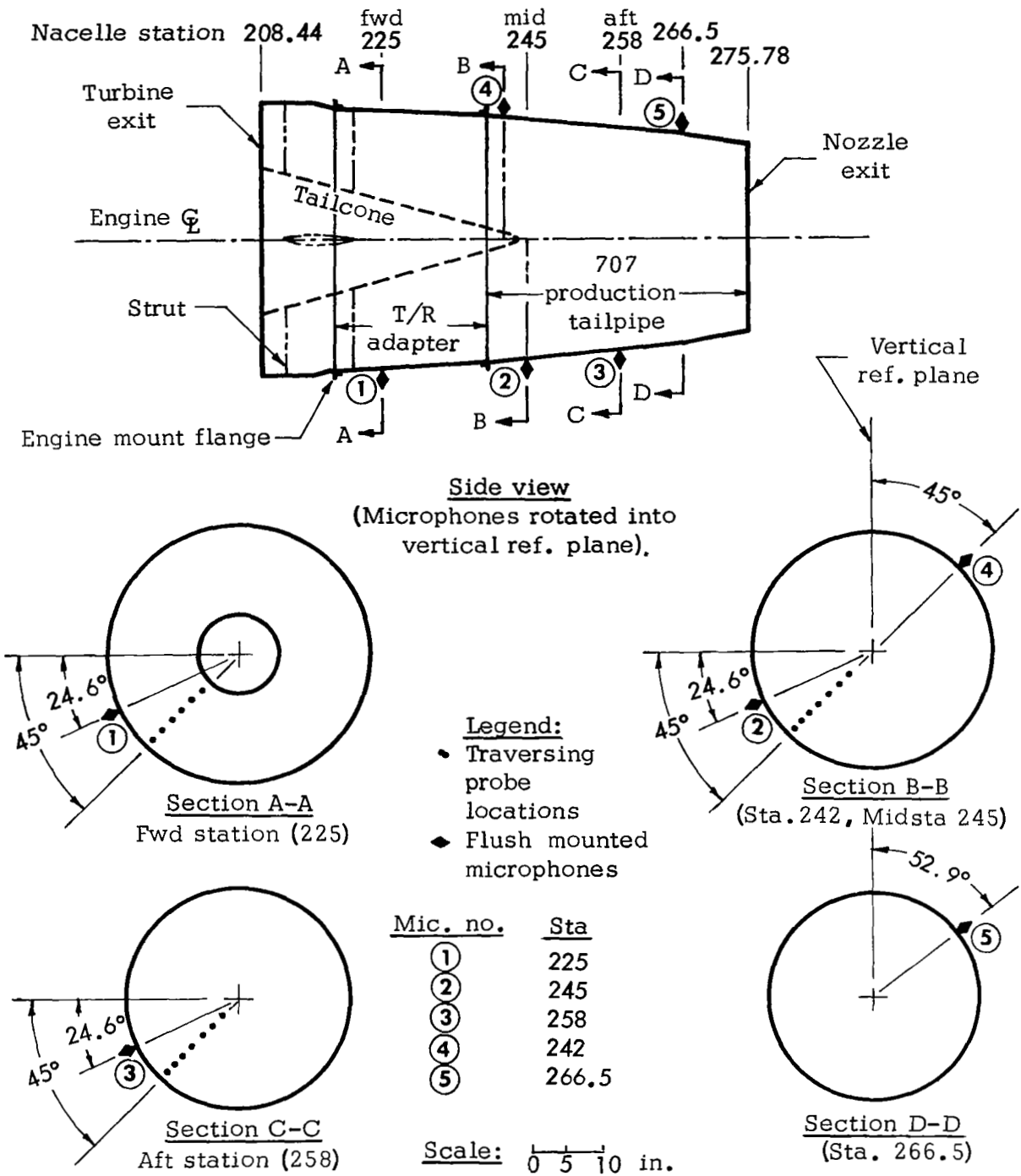


Figure 4. Aeroacoustic instrumentation, baseline tailpipe

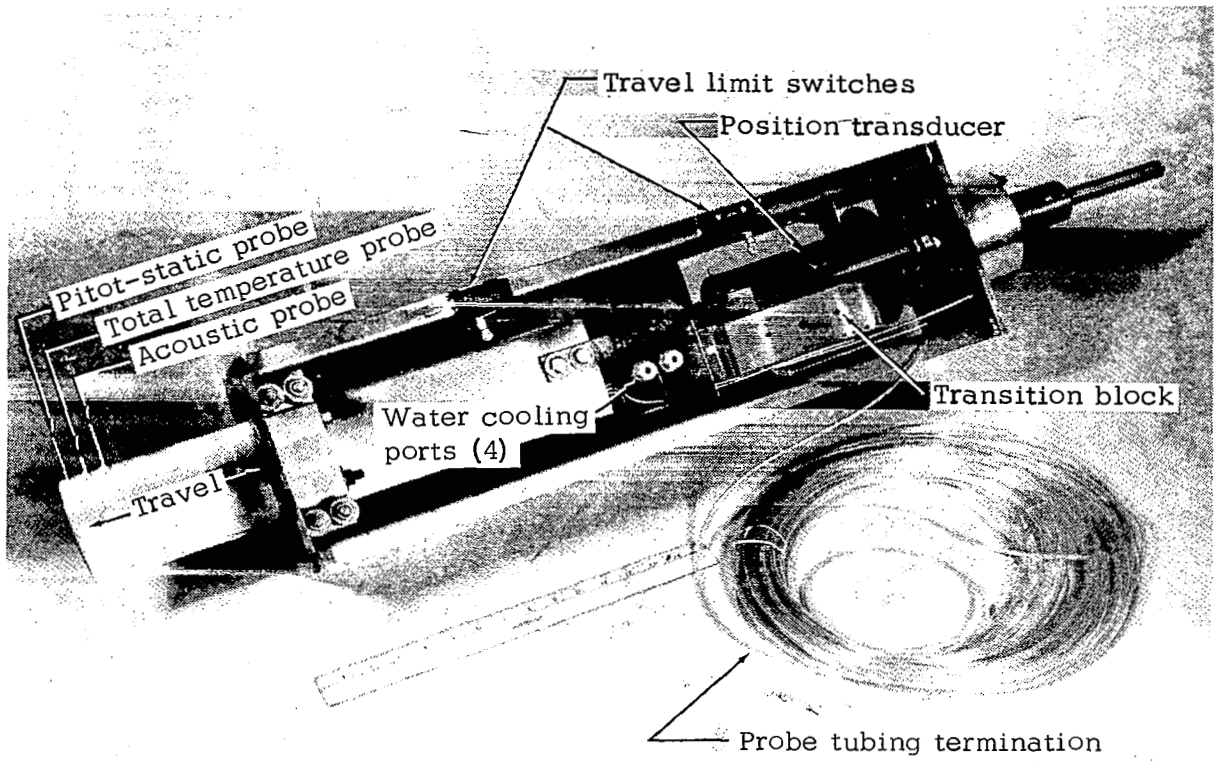


Figure 5. Tailpipe internal survey traversing probe assembly

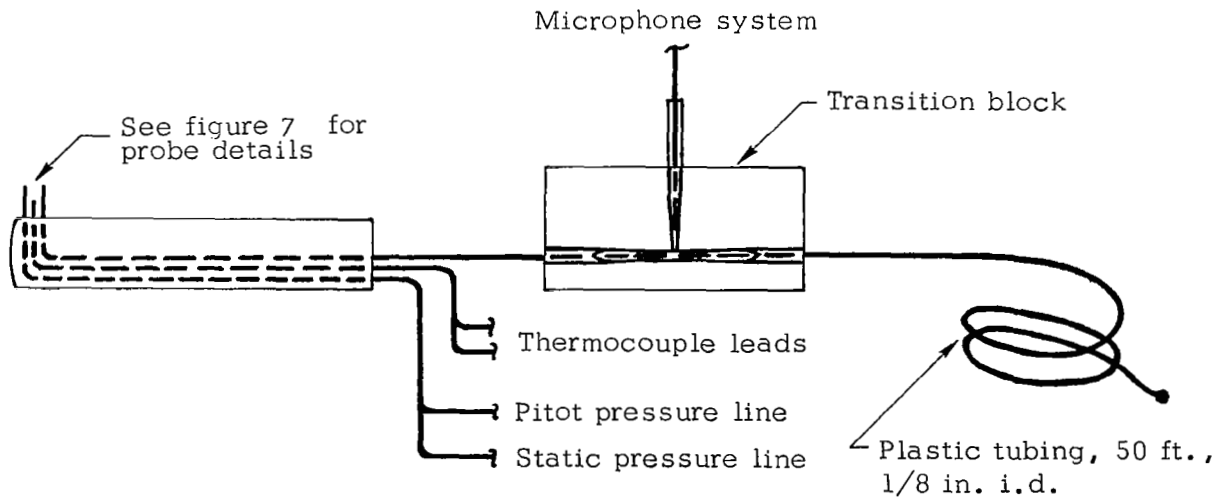


Figure 6. Schematic of traversing probe assembly

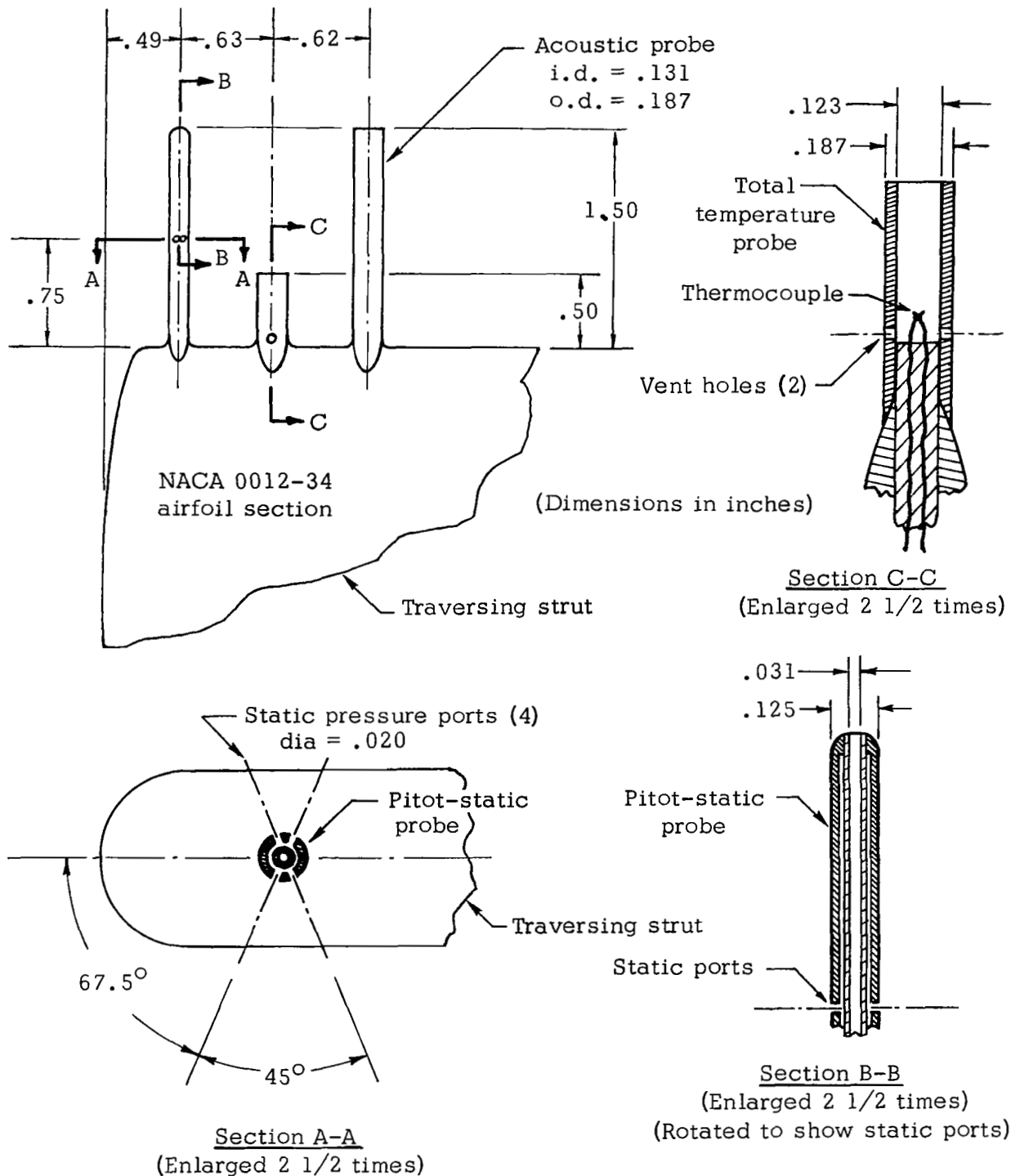
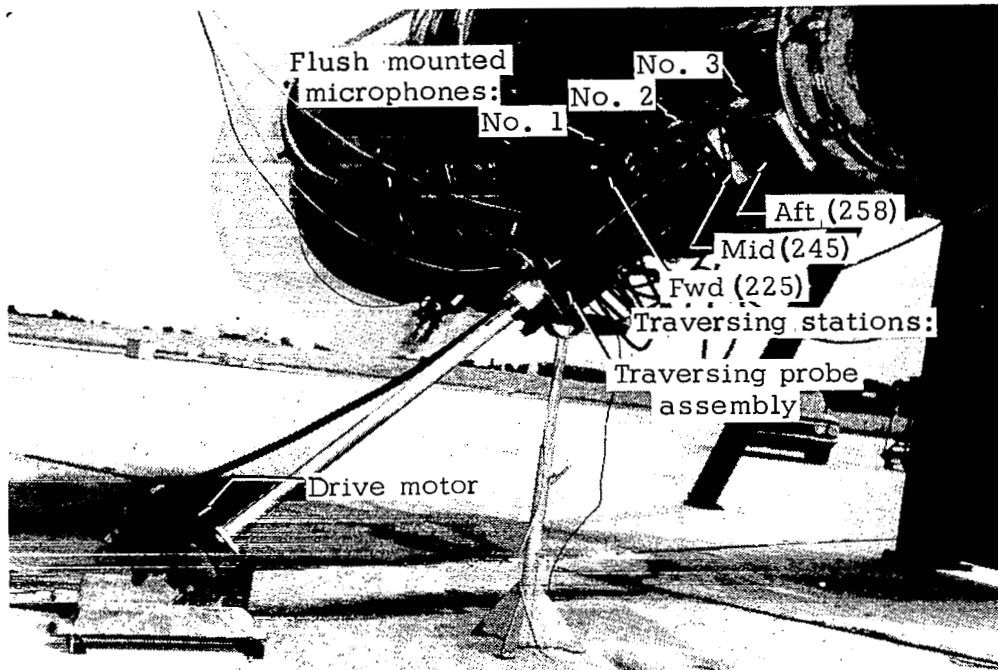
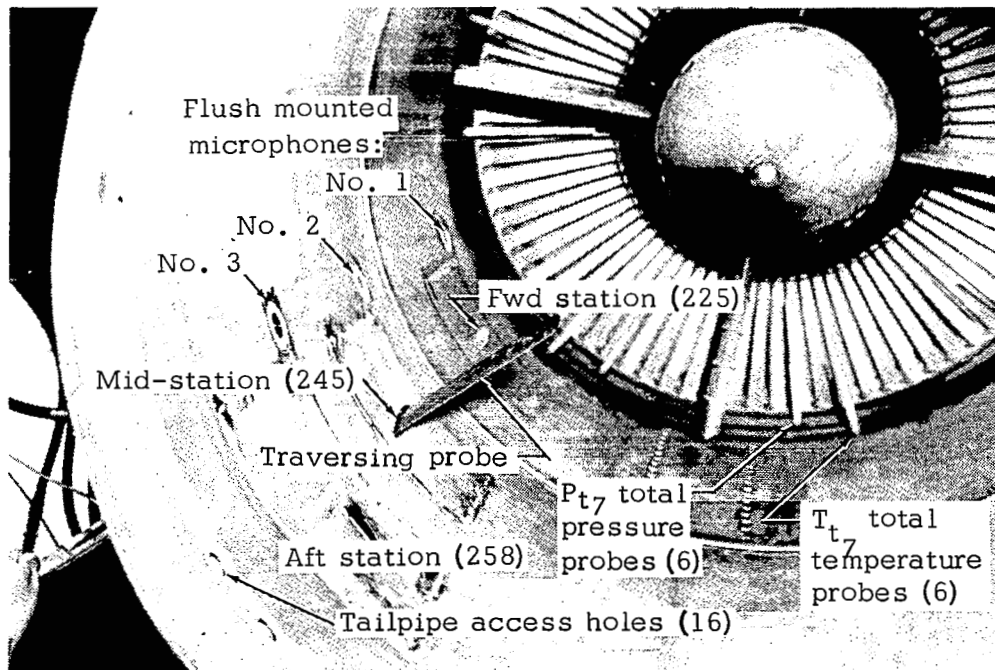


Figure 7. Aeroacoustic traversing probe details



(a) External view of tailpipe



(b) Internal view of tailpipe

Figure 8. Tailpipe internal survey instrumentation

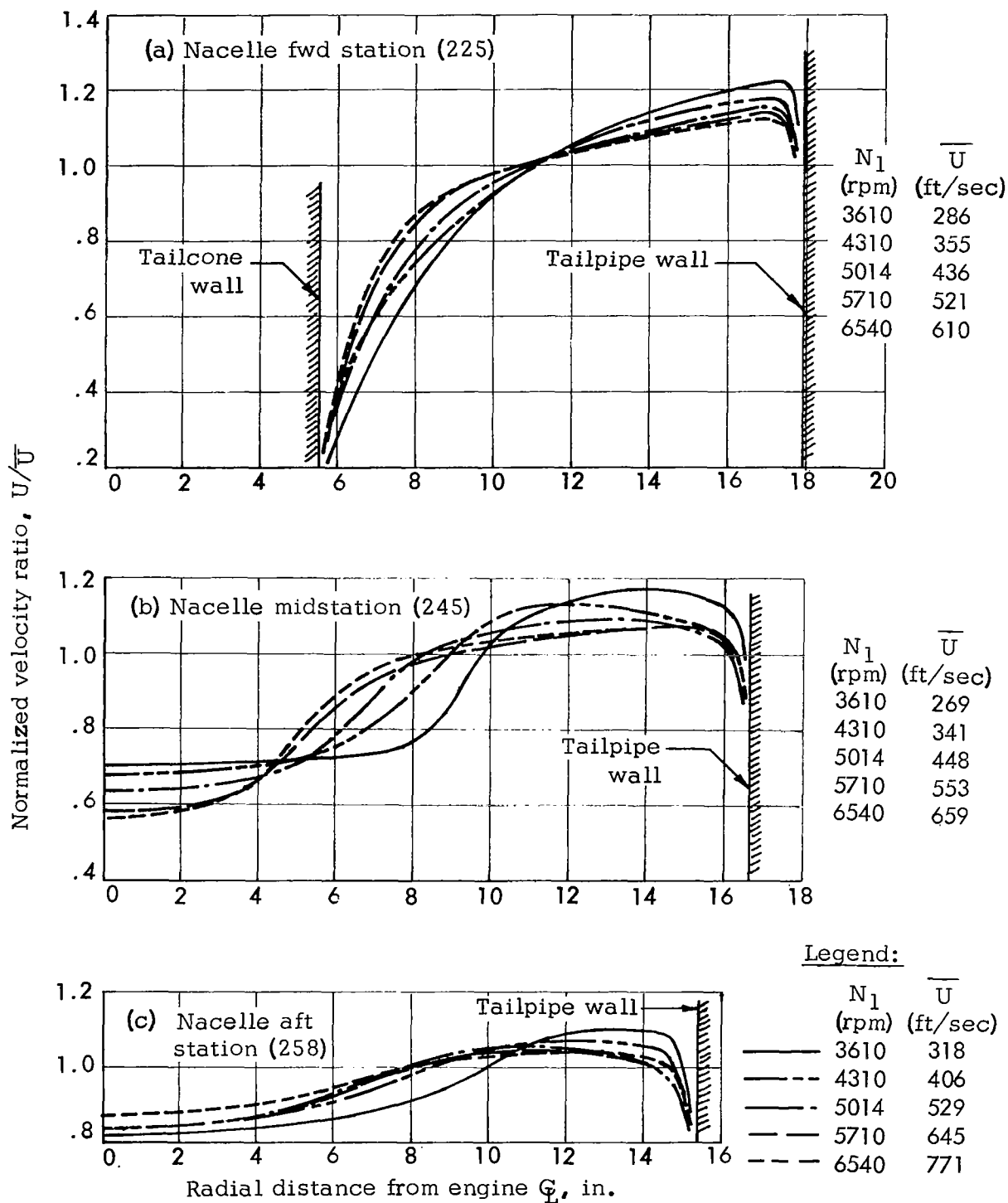


Figure 9. Velocity survey, baseline tailpipe

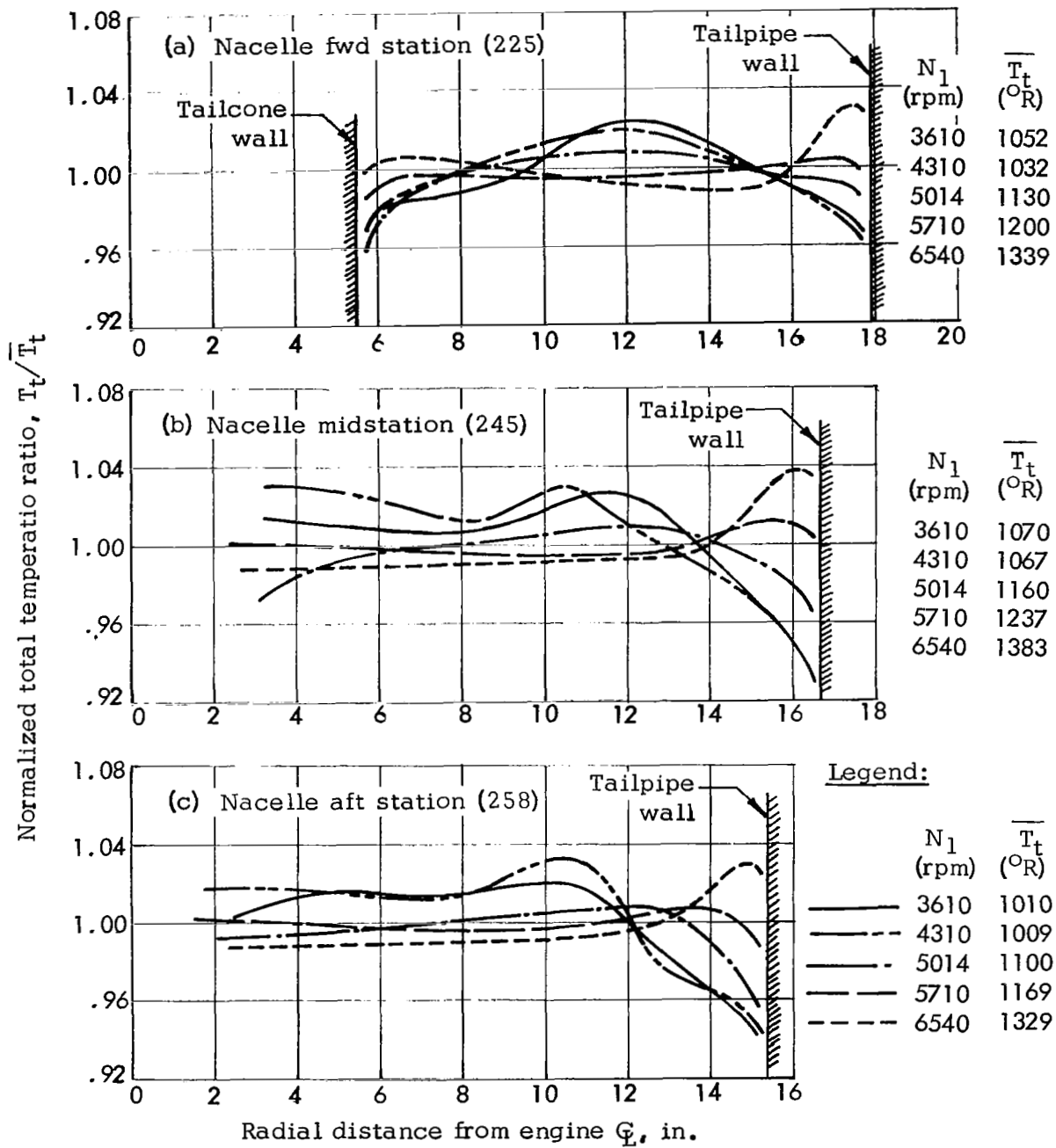
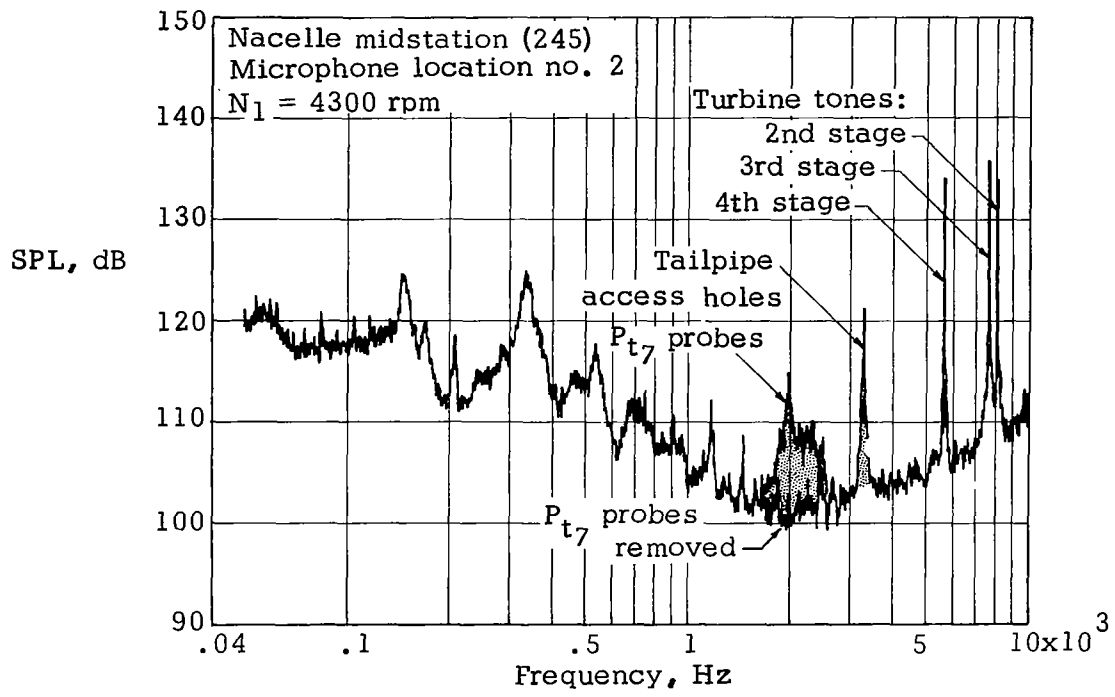
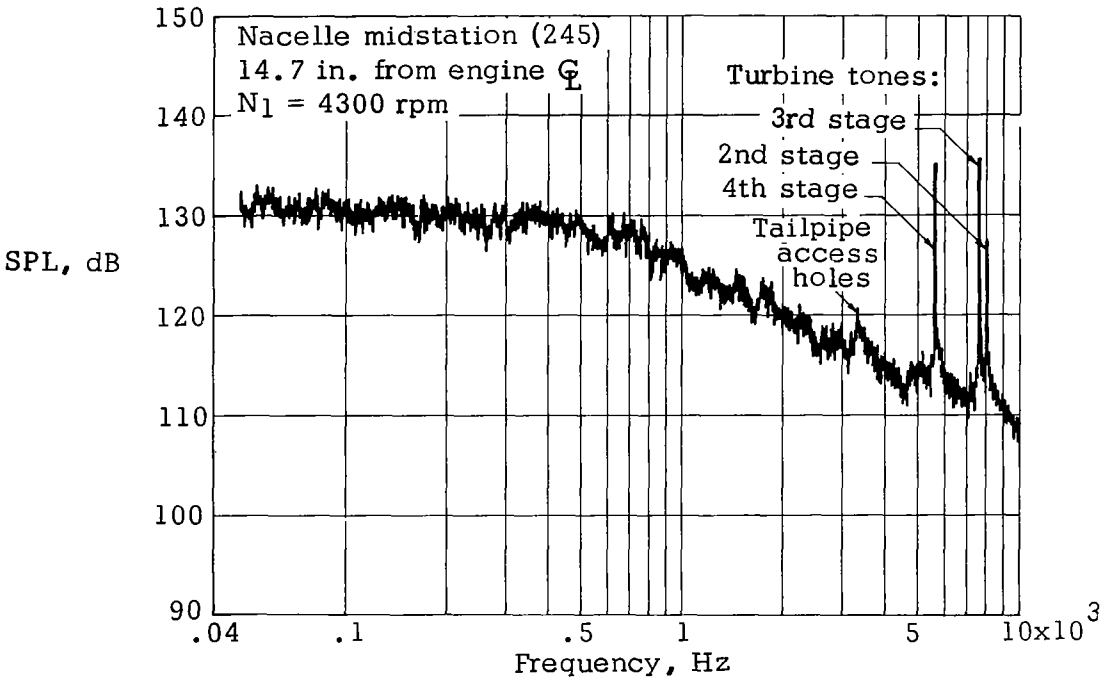


Figure 10. Total temperature survey, baseline tailpipe

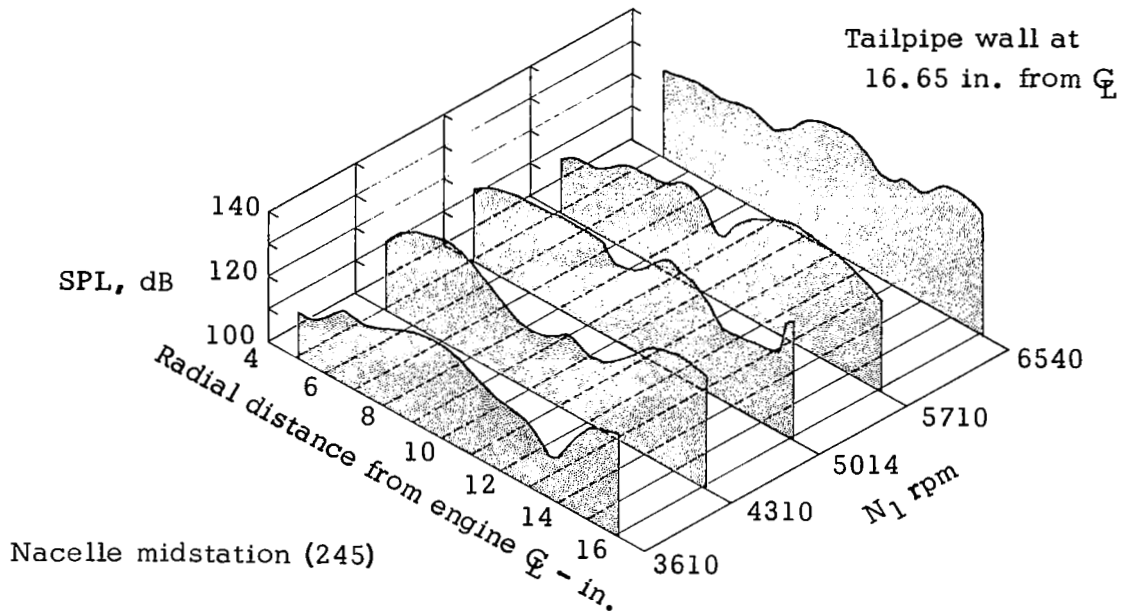


(a) Flush mounted microphone spectra

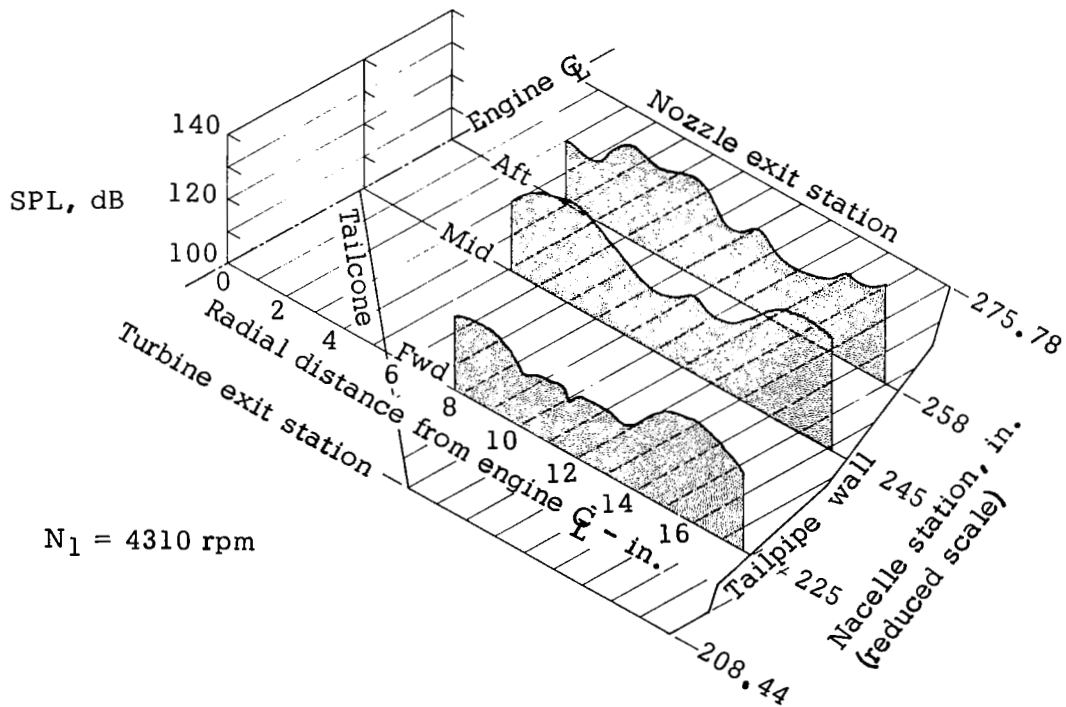


(b) Probe microphone spectrum

Figure 11. Acoustic survey, baseline tailpipe



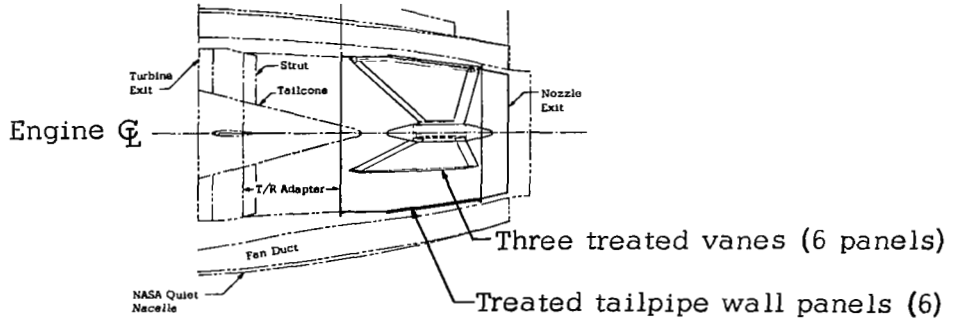
(a) Effect of engine power setting



(b) Variation with nacelle station

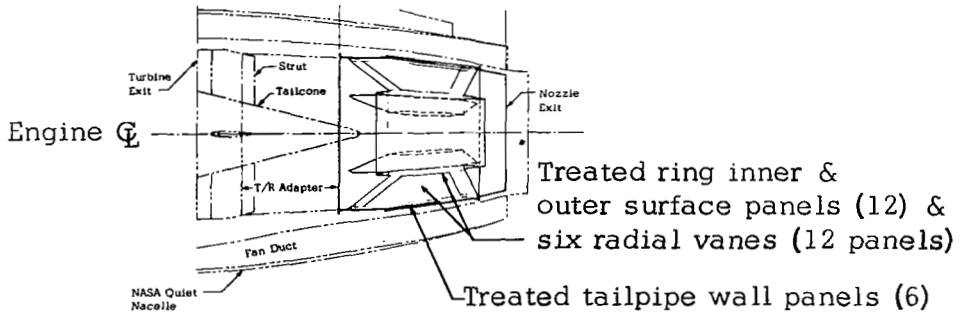
Figure 12. Fourth stage turbine tone survey

Nacelle station 208.44 239.612 275.78



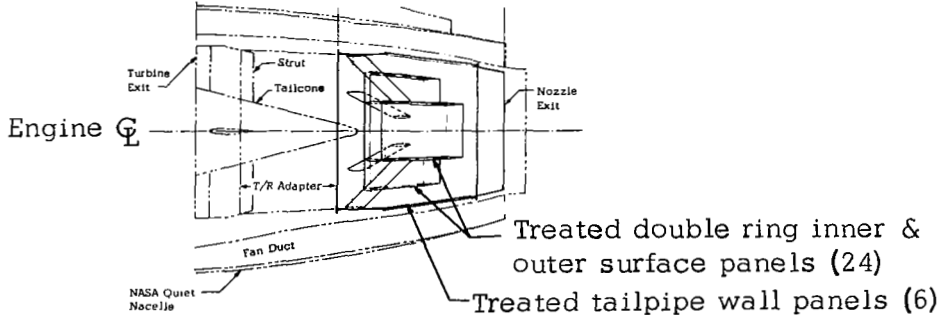
(a) Radial vanes

Nacelle station 208.44 239.612 275.78



(b) Ring with radial vanes

Nacelle station 208.44 239.612 275.78



(c) Two rings

0 10 in.
Scale

Figure 13. Tailpipe lining concepts

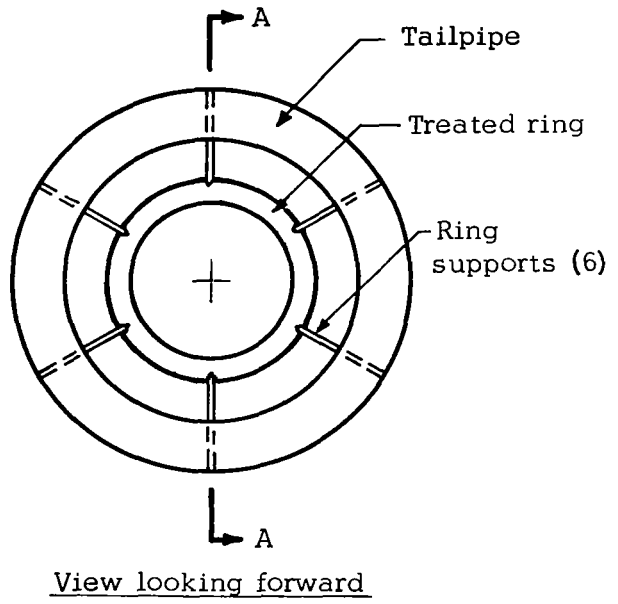
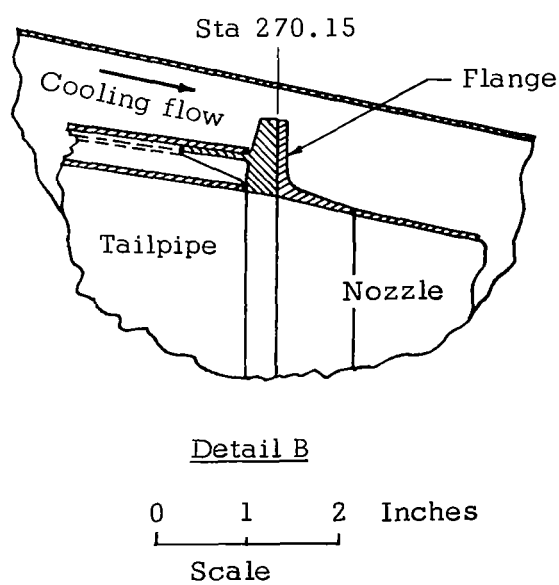
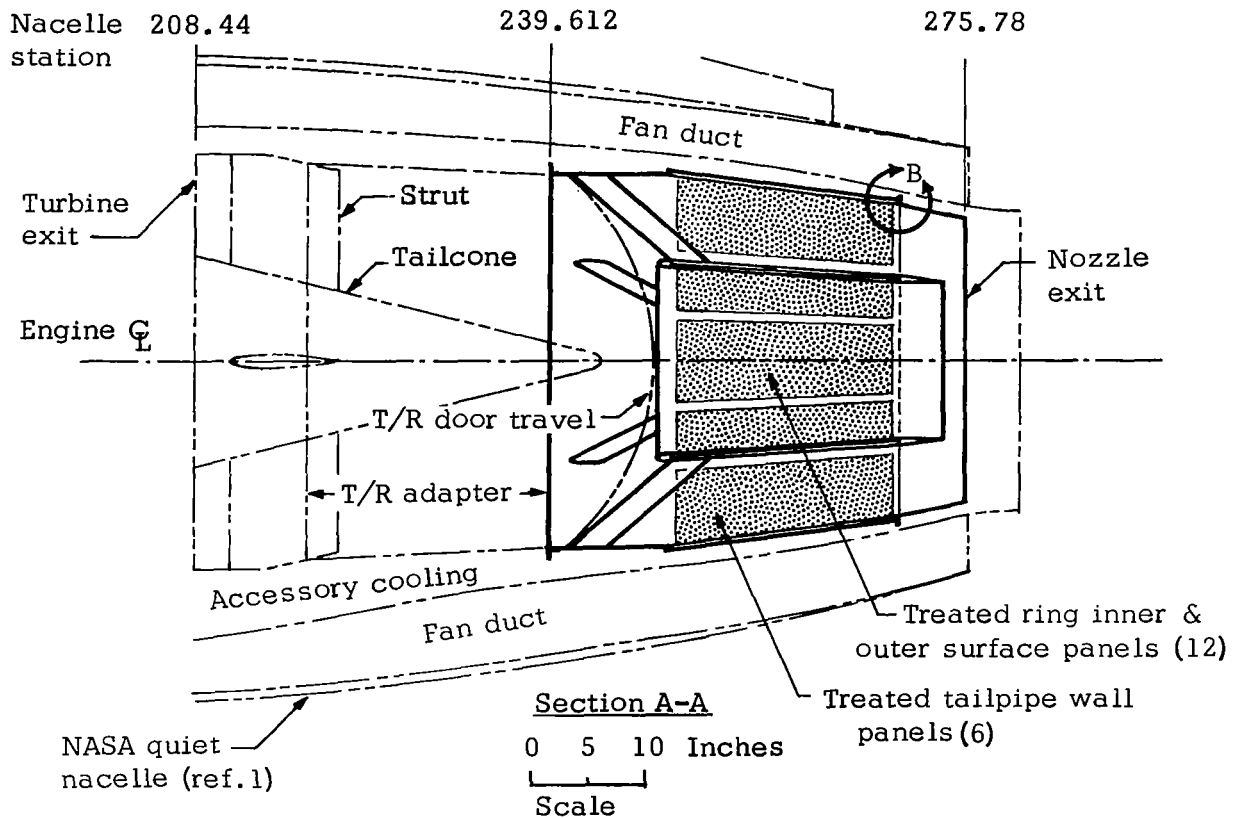
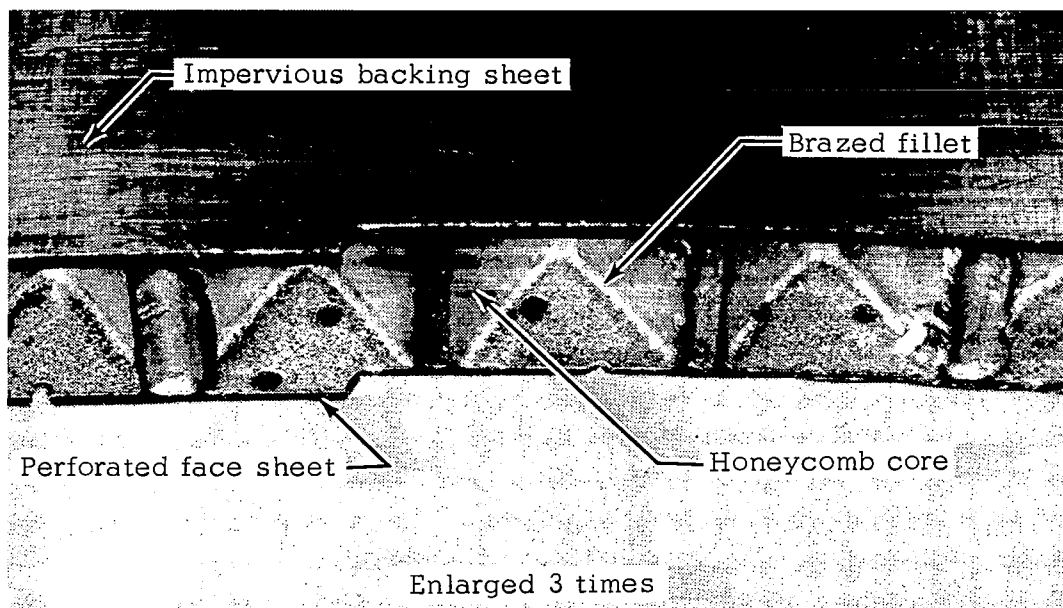
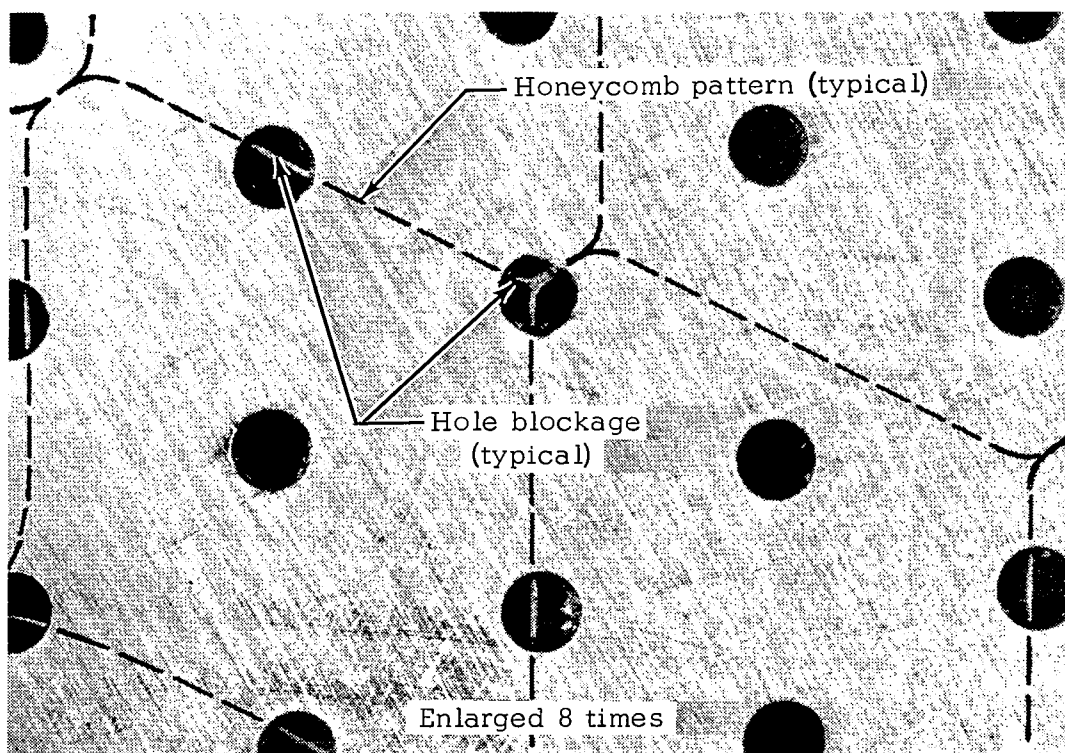


Figure 14. Single-ring treated tailpipe assembly



(a) Furnace-brazed stainless steel panel construction



(b) Hole blockage due to honeycomb core

Figure 15. Typical perforated sheet acoustic panel

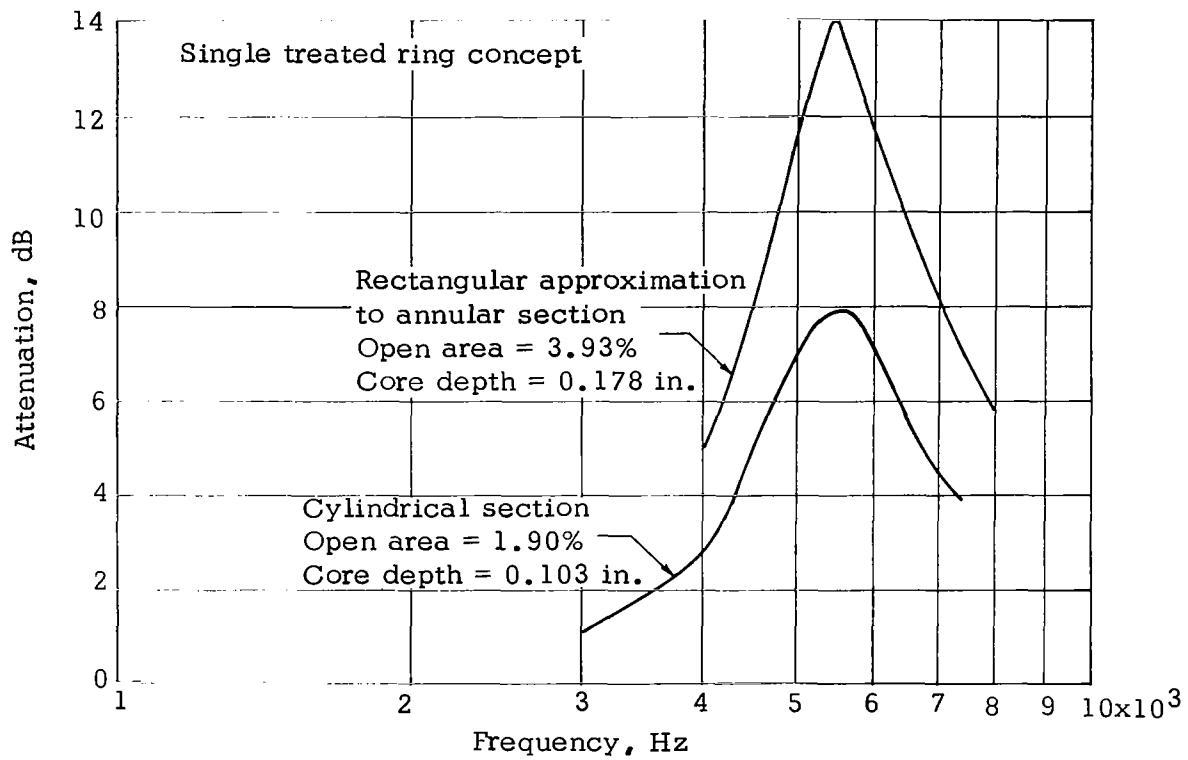
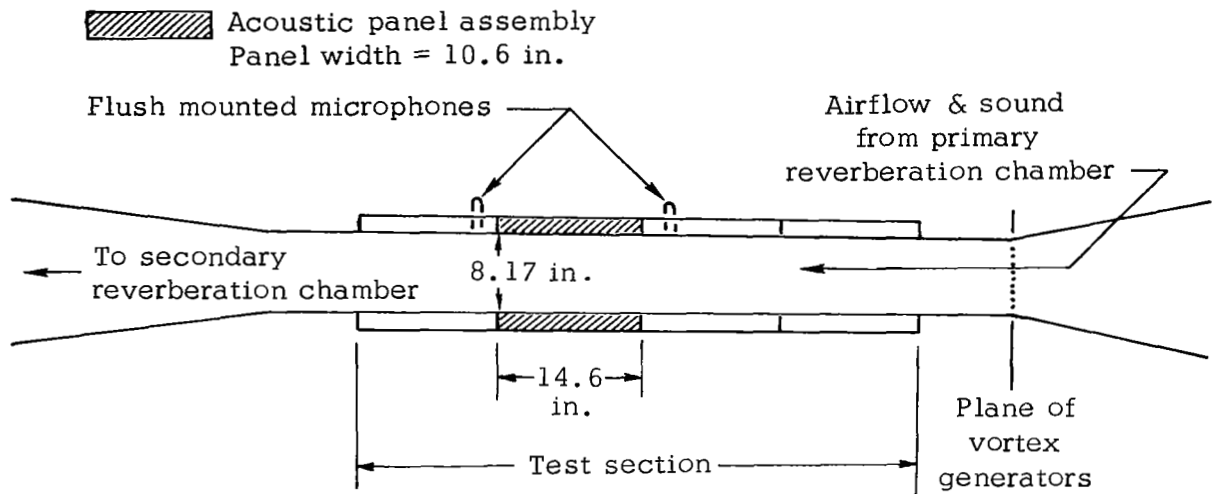
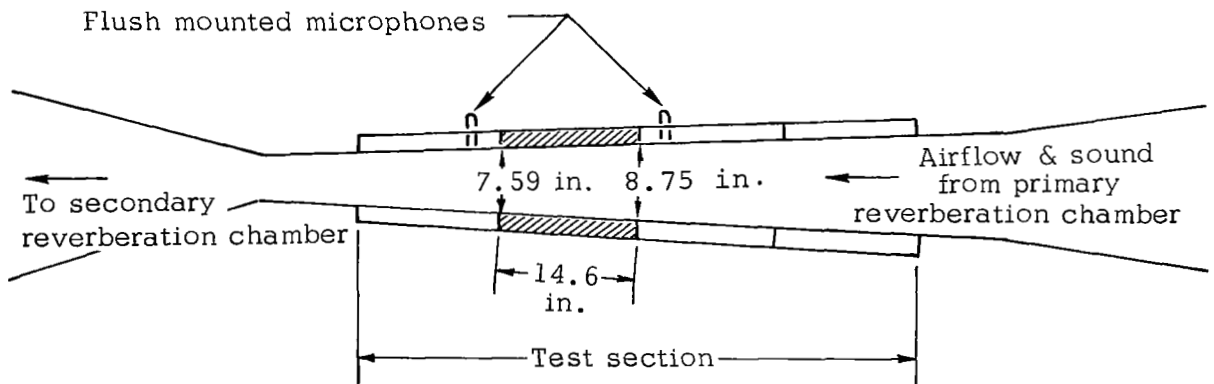


Figure 16. Predicted attenuation for perforated sheet lining



(a) Constant area duct



(b) Convergent duct

Figure 17. Flow duct configurations

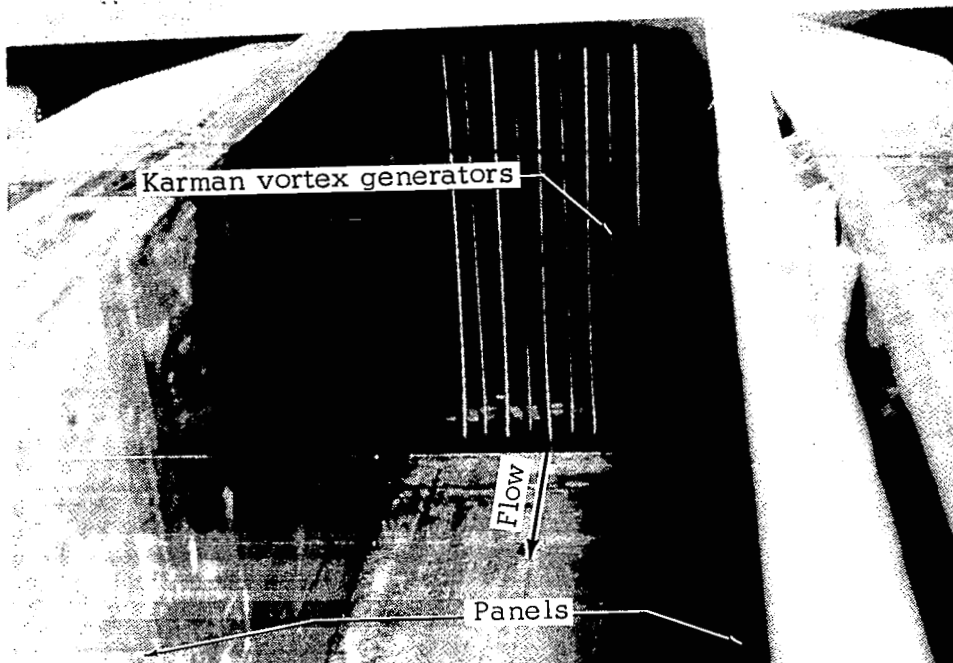


Figure 18. Flow duct turbine tone simulation

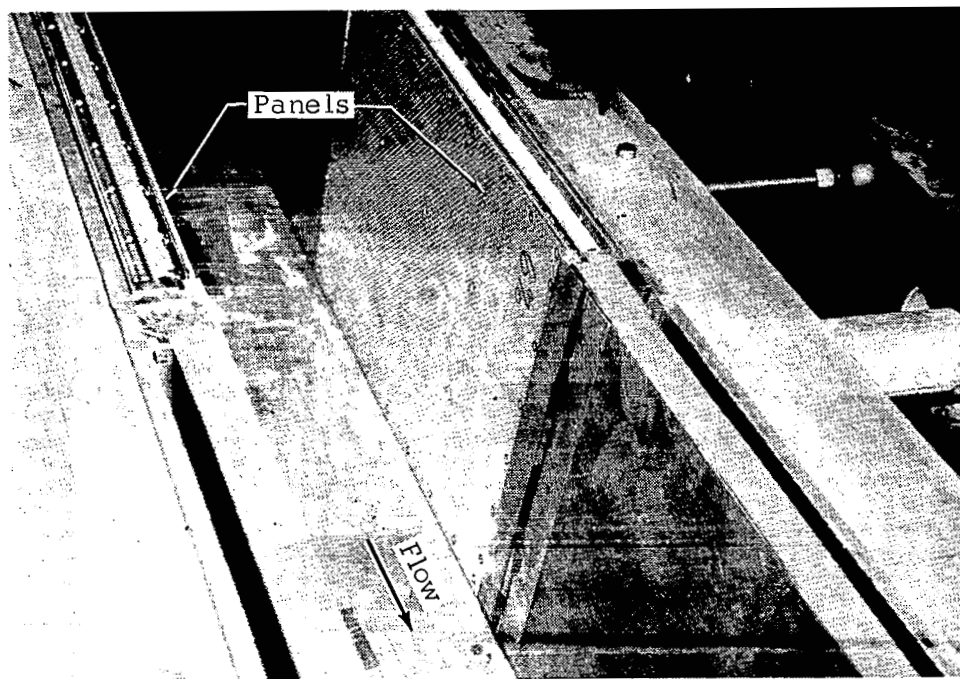


Figure 19. Flow duct acoustic panels installed

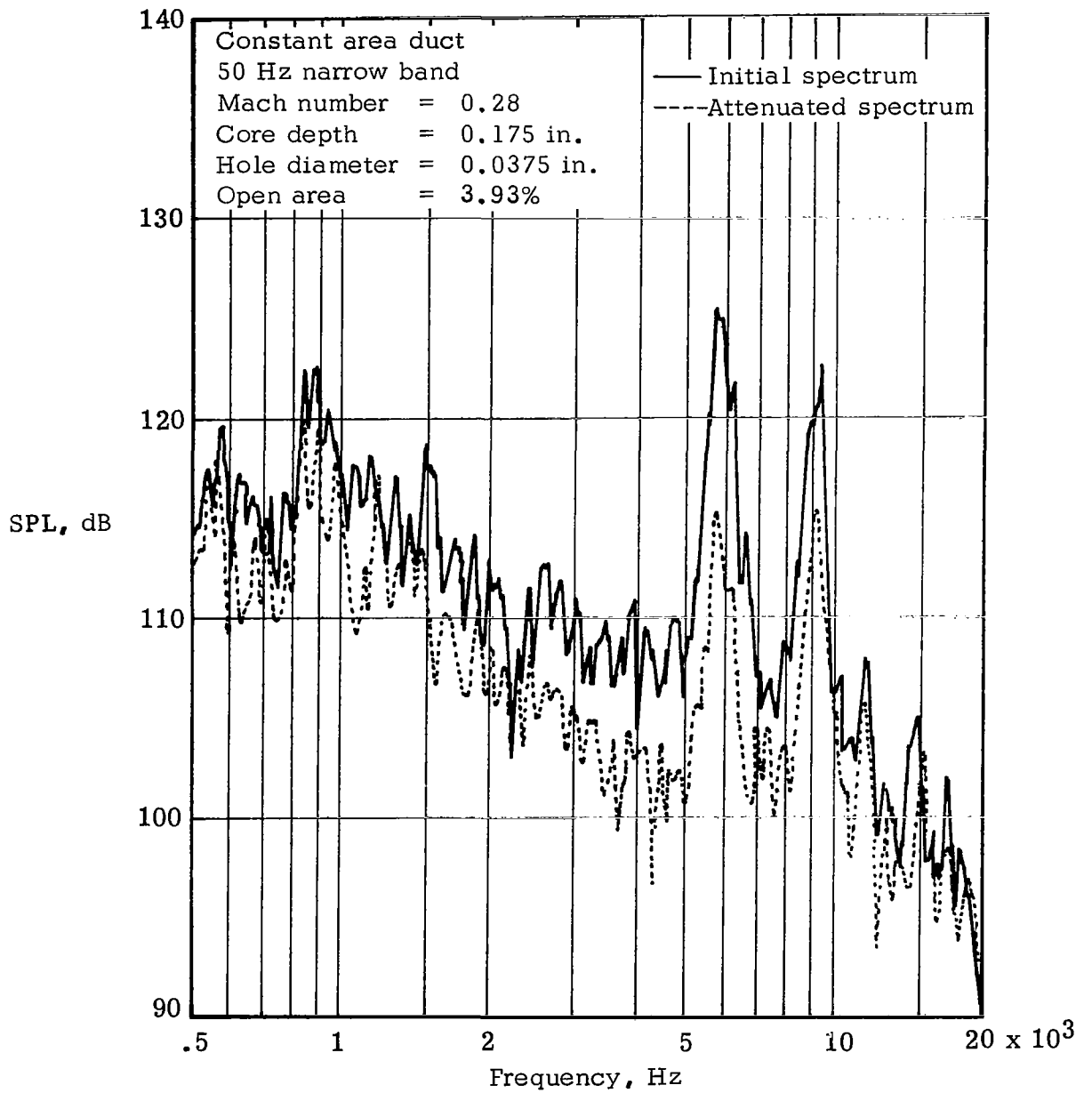


Figure 20. Flow duct noise spectra, simulated turbine tone

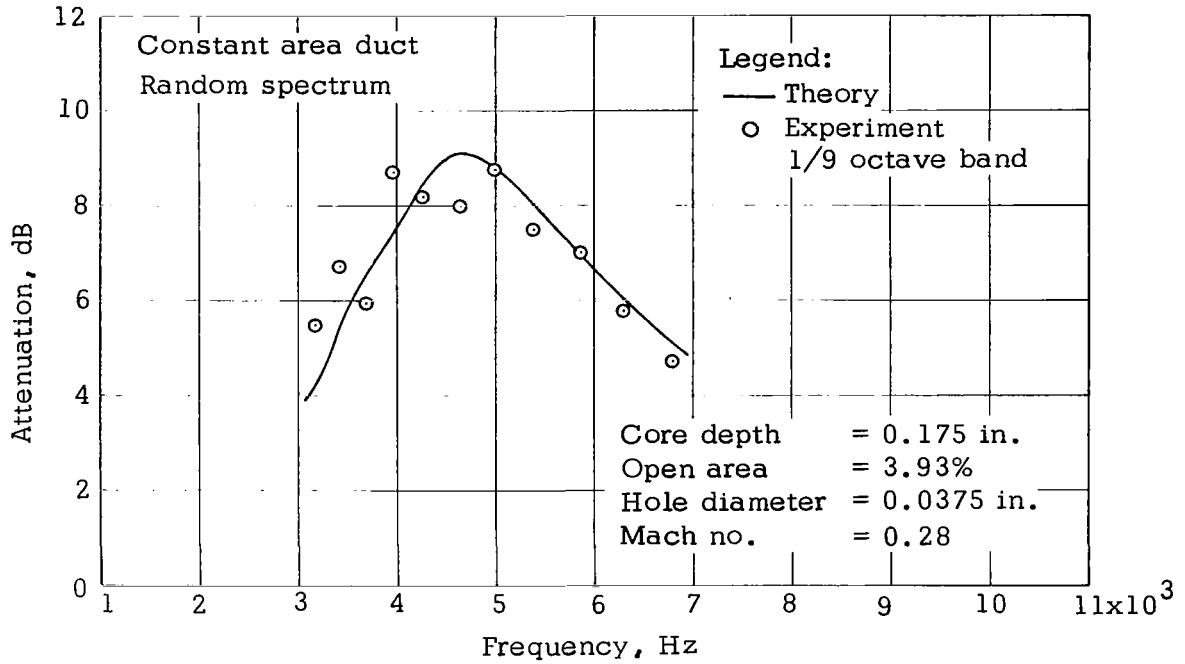


Figure 21. Comparison of analytical predictions with flow duct test results

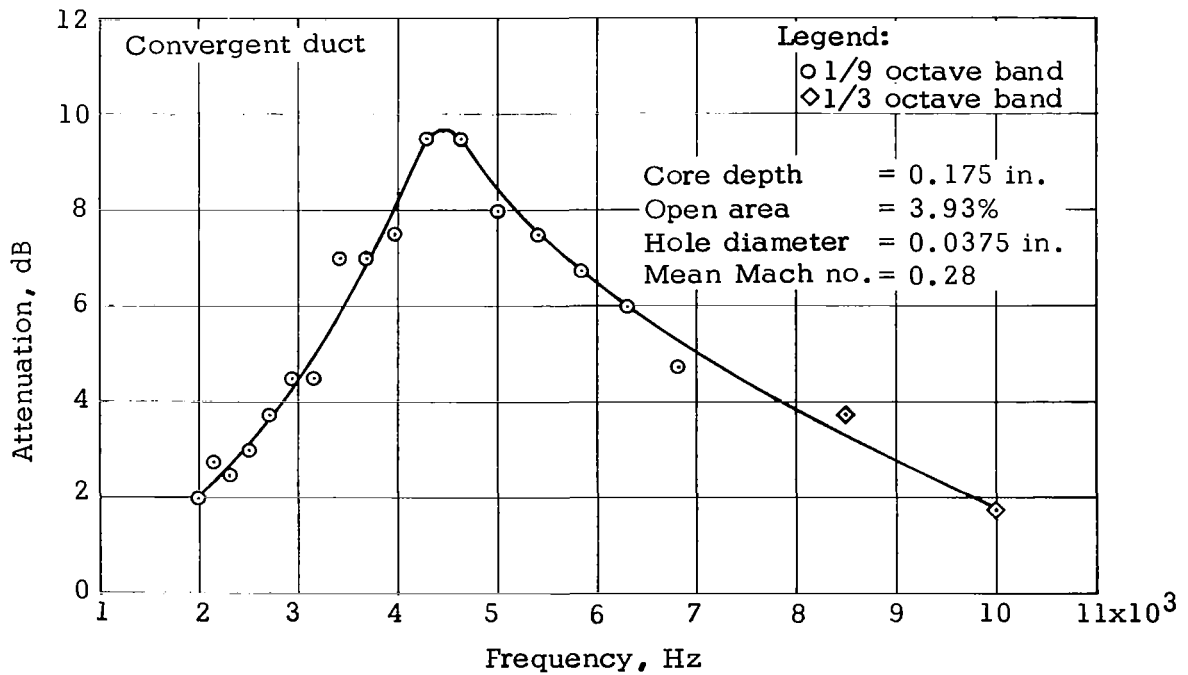


Figure 22. Flow duct random noise attenuation

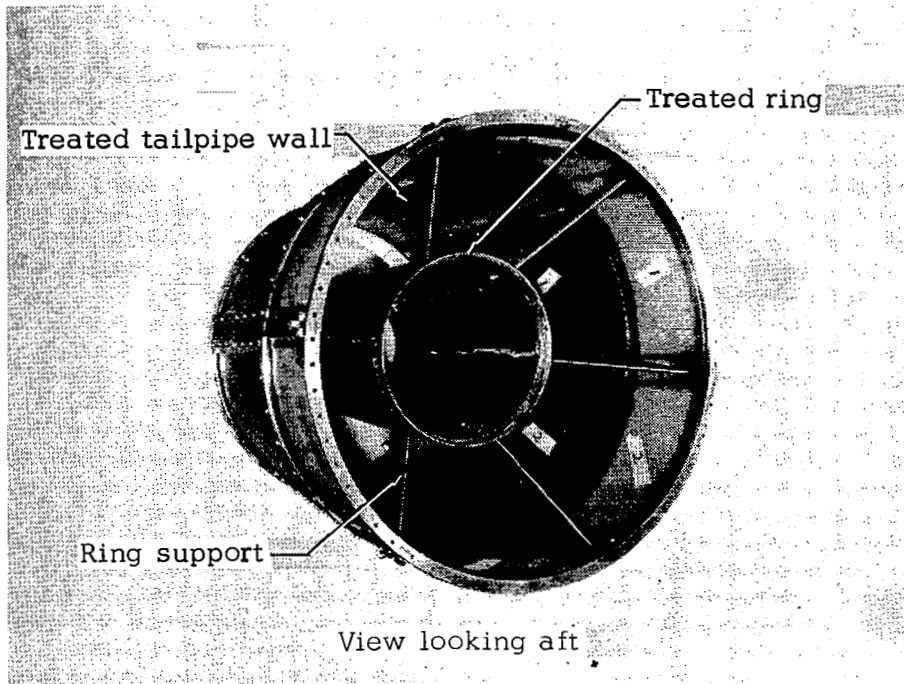


Figure 23. Treated tailpipe assembly

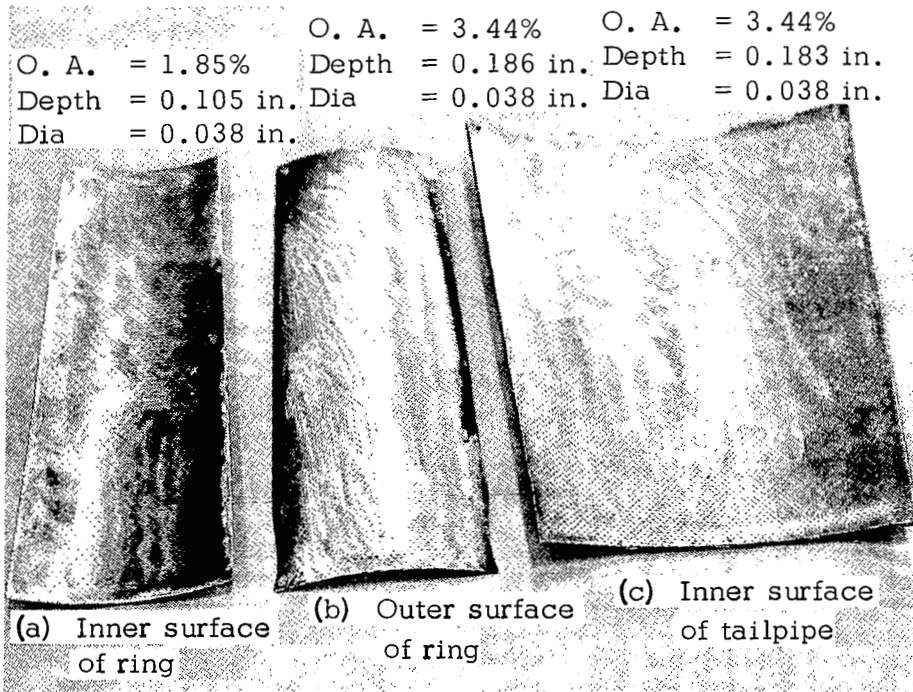


Figure 24. Furnace-brazed, stainless steel, acoustic panels

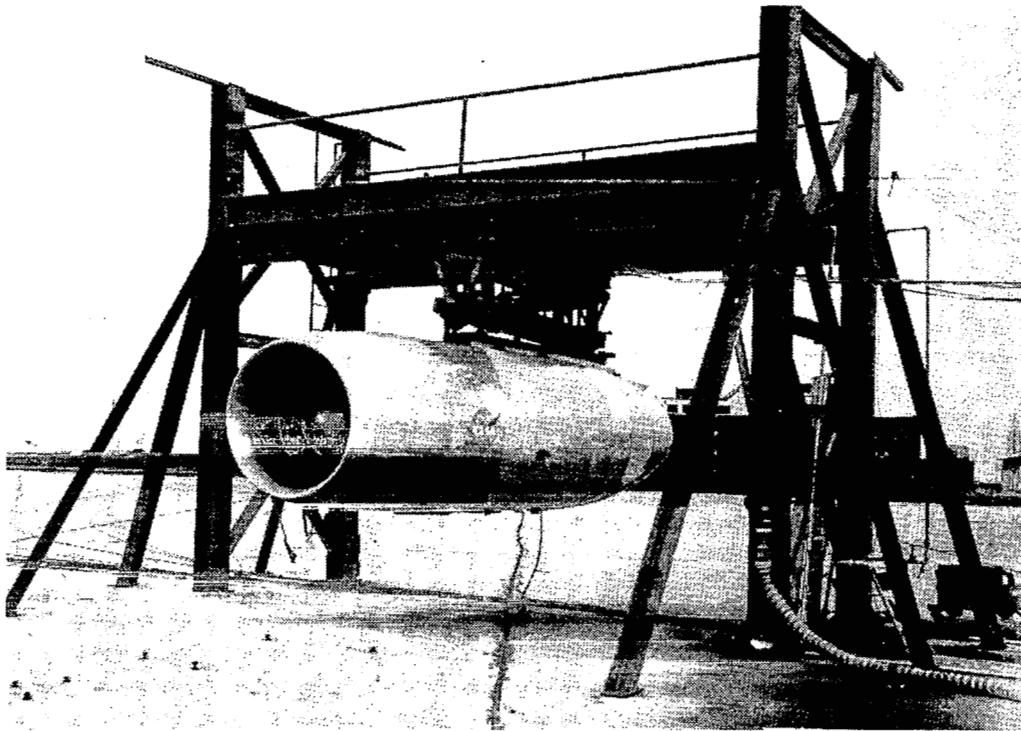


Figure 25. NASA flightworthy quiet nacelle installed on JT3D-3B engine

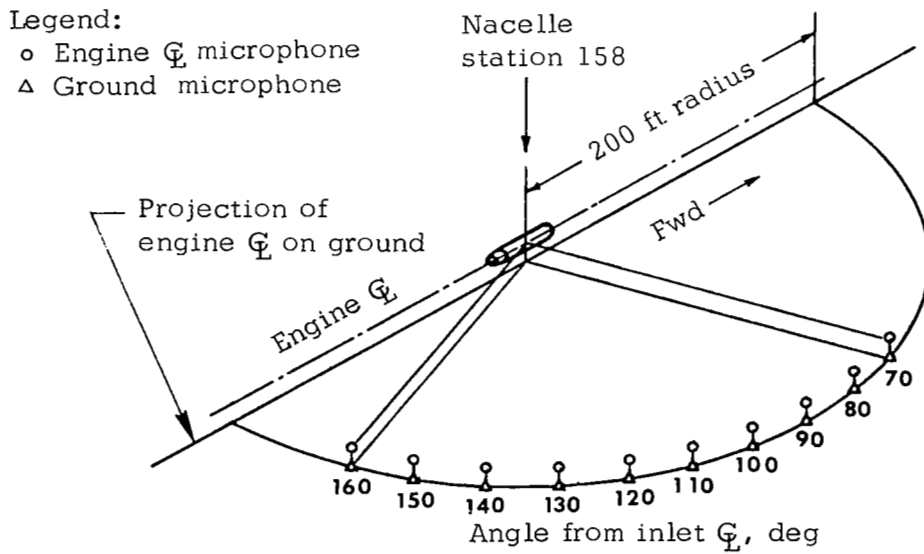
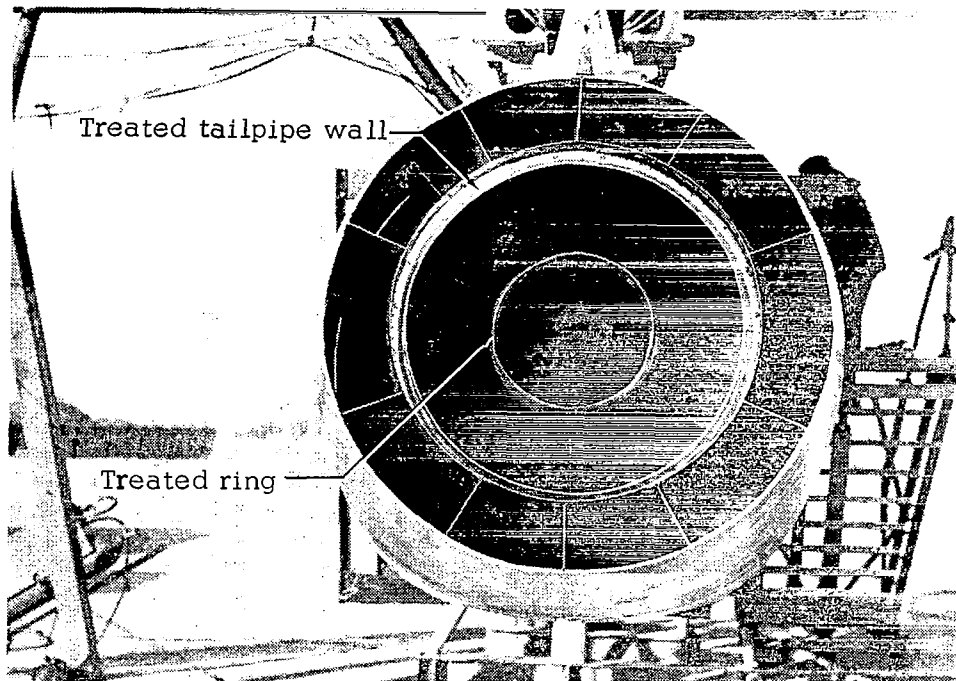
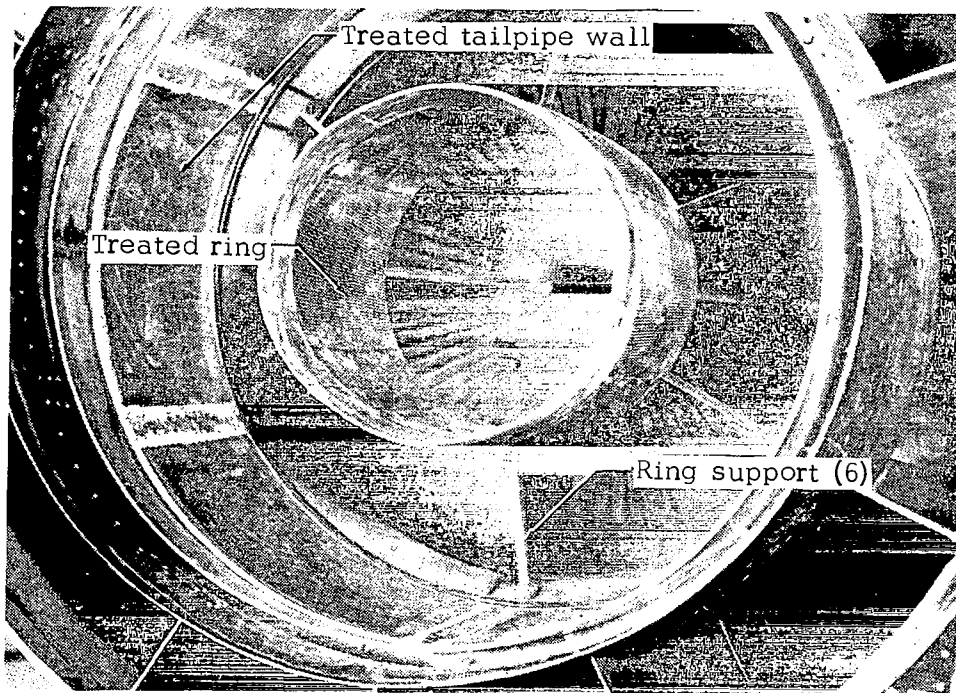


Figure 26. Far field microphone polar array



(a) Aft view of tailpipe



(b) Internal view of tailpipe

Figure 27. Treated tailpipe installation

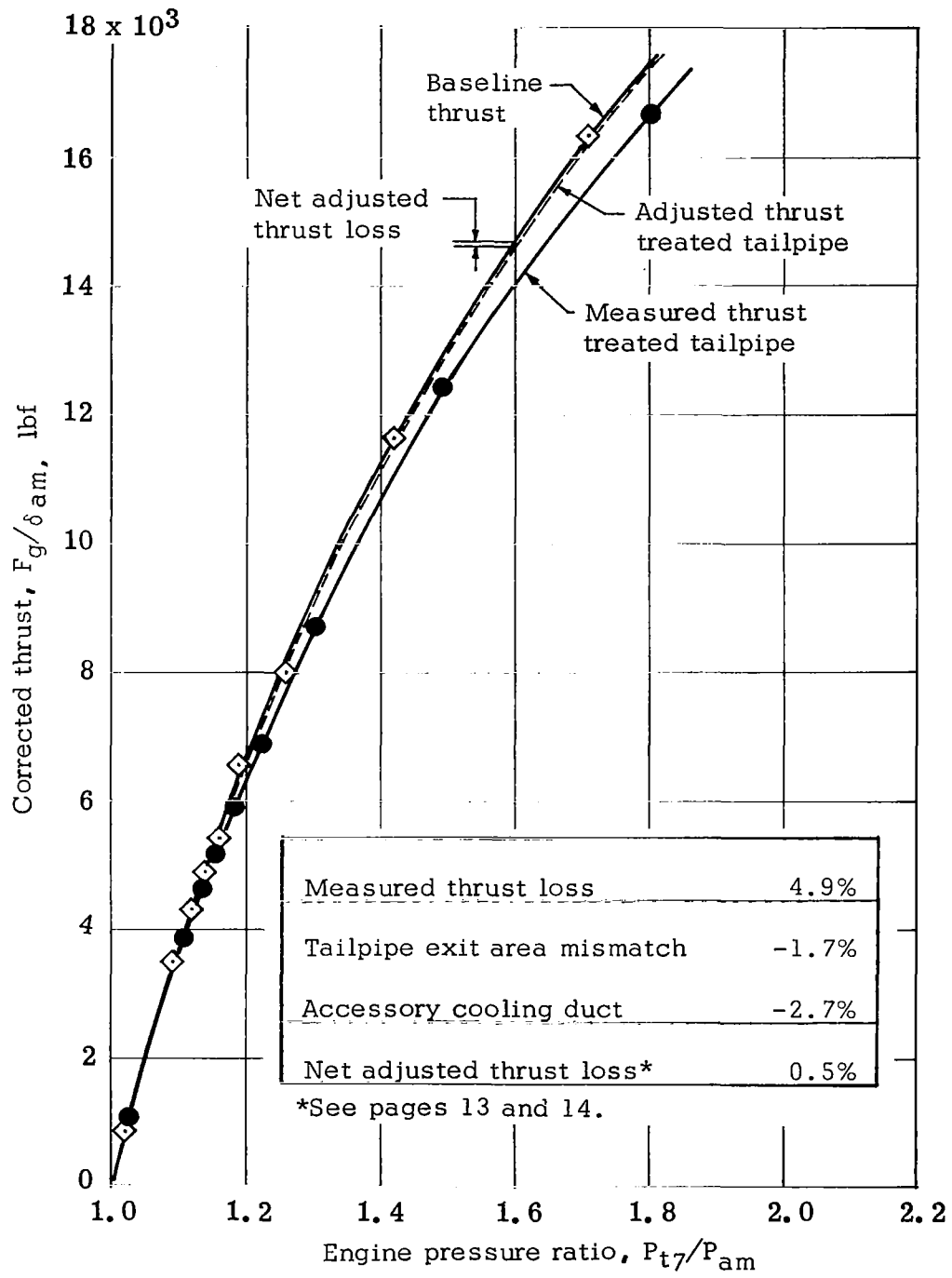


Figure 28. Effect of treated tailpipe on engine thrust

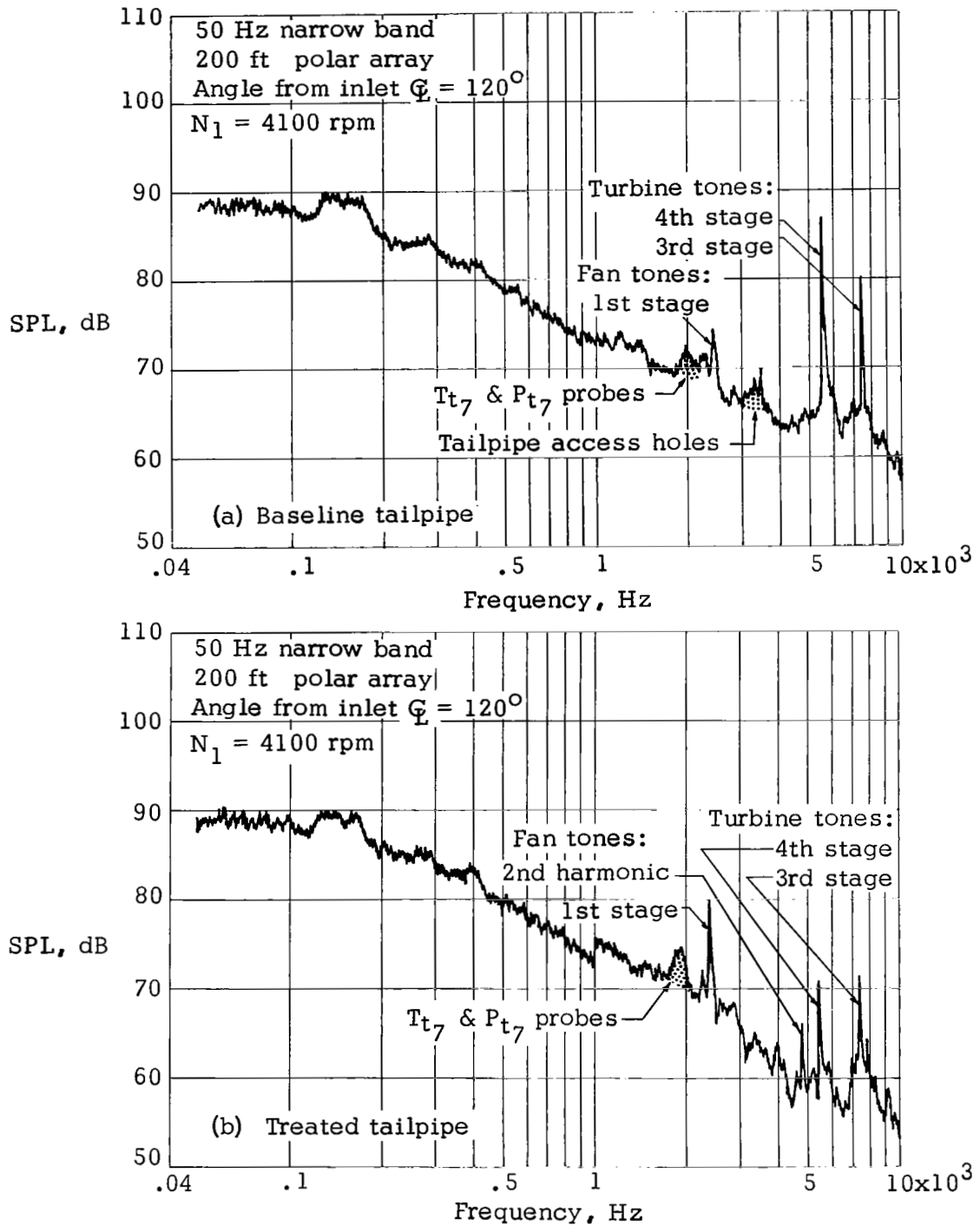


Figure 29. Far field noise spectra from ground microphone

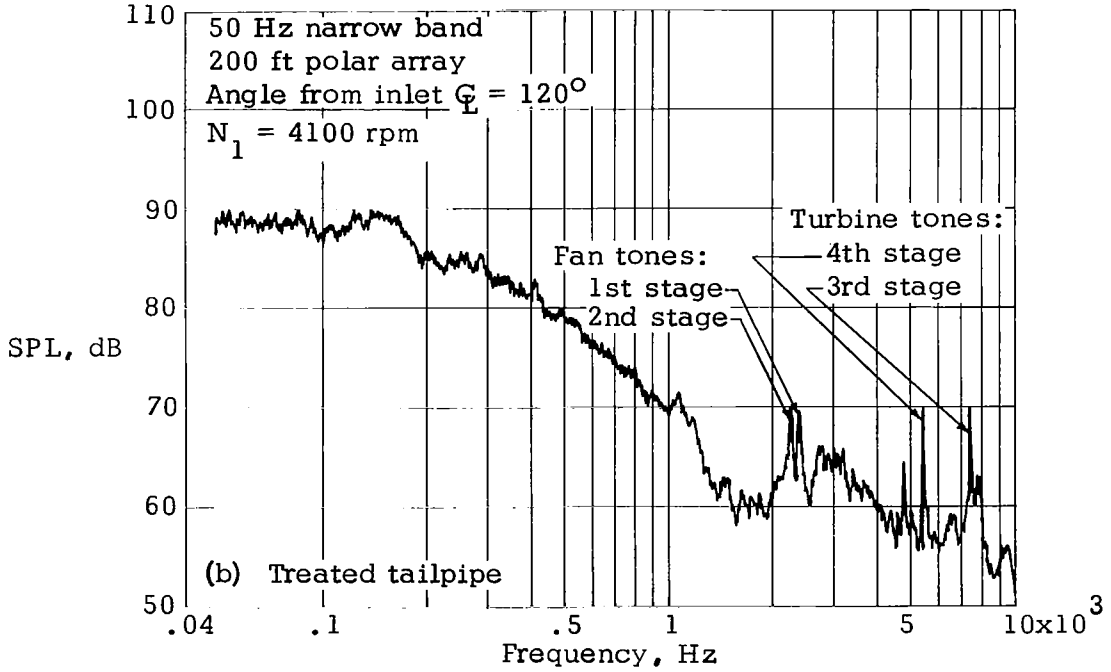
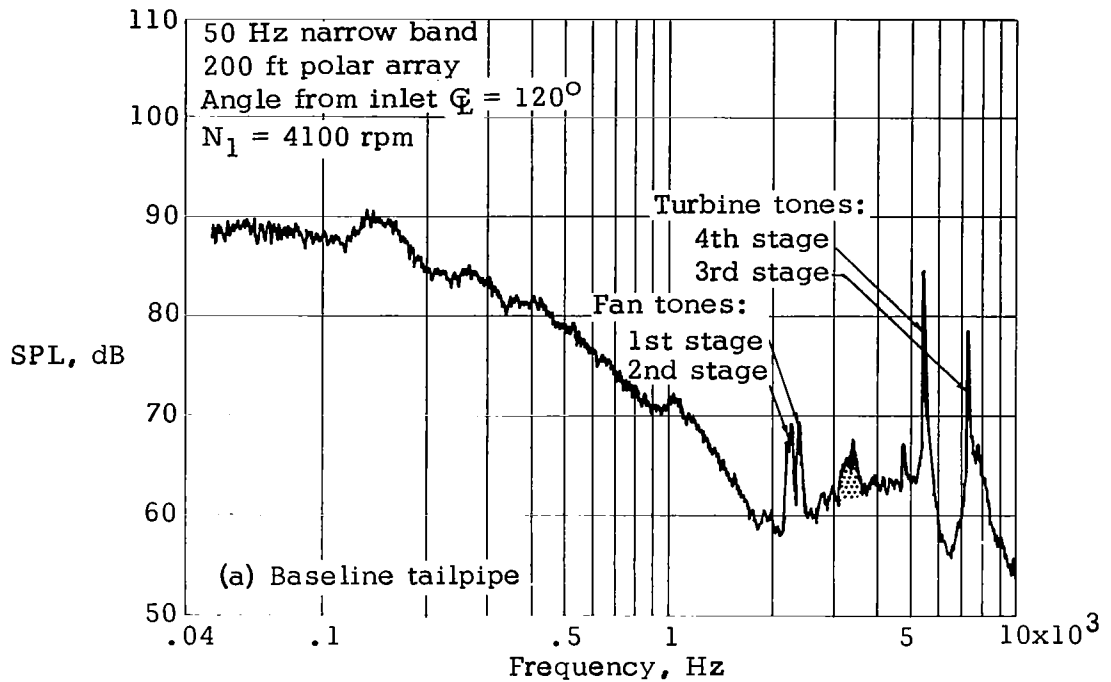


Figure 30. Far field noise spectra from engine ϕ microphone

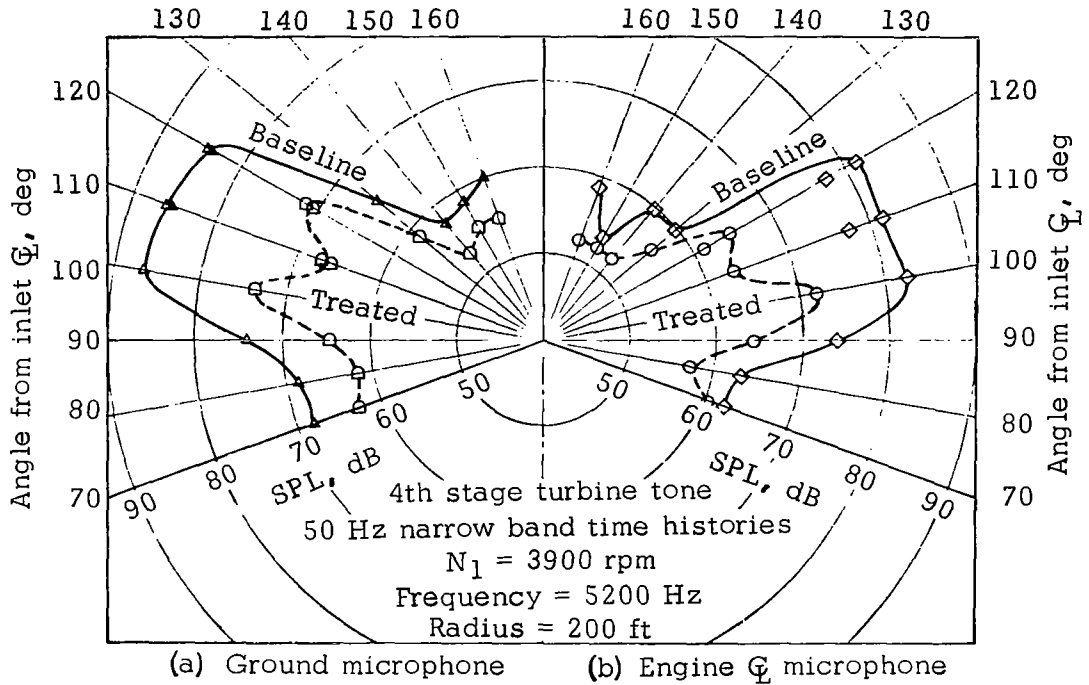


Figure 31. Microphone height effect on 4th stage turbine tone measurements

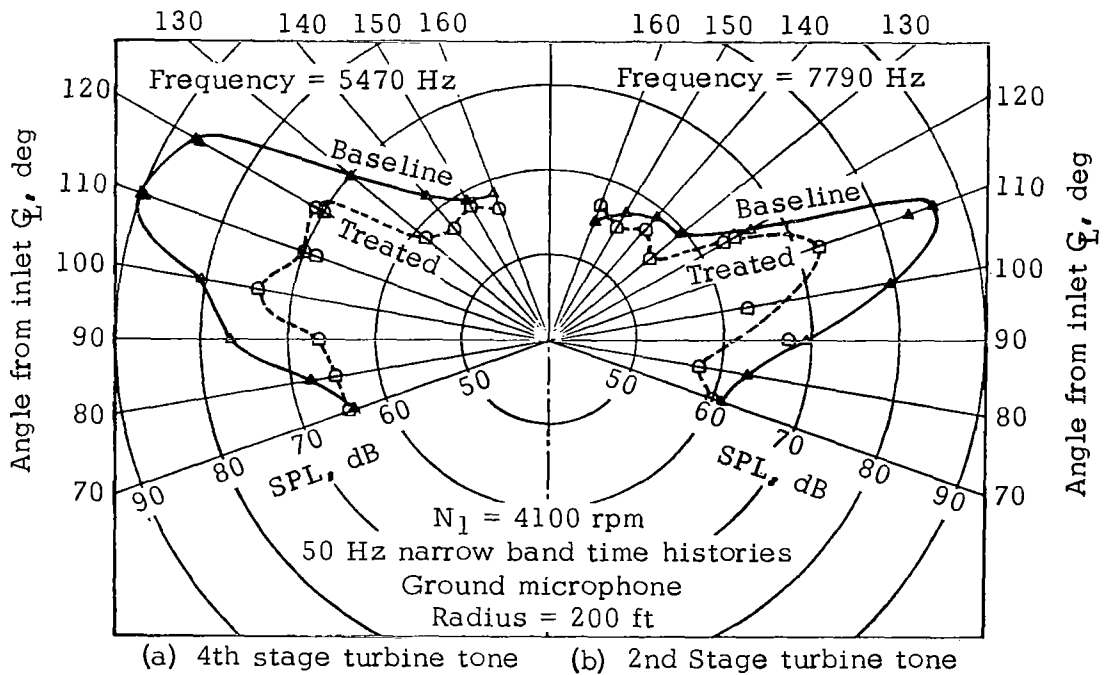


Figure 32. Comparison of 2nd and 4th stage turbine tone suppression

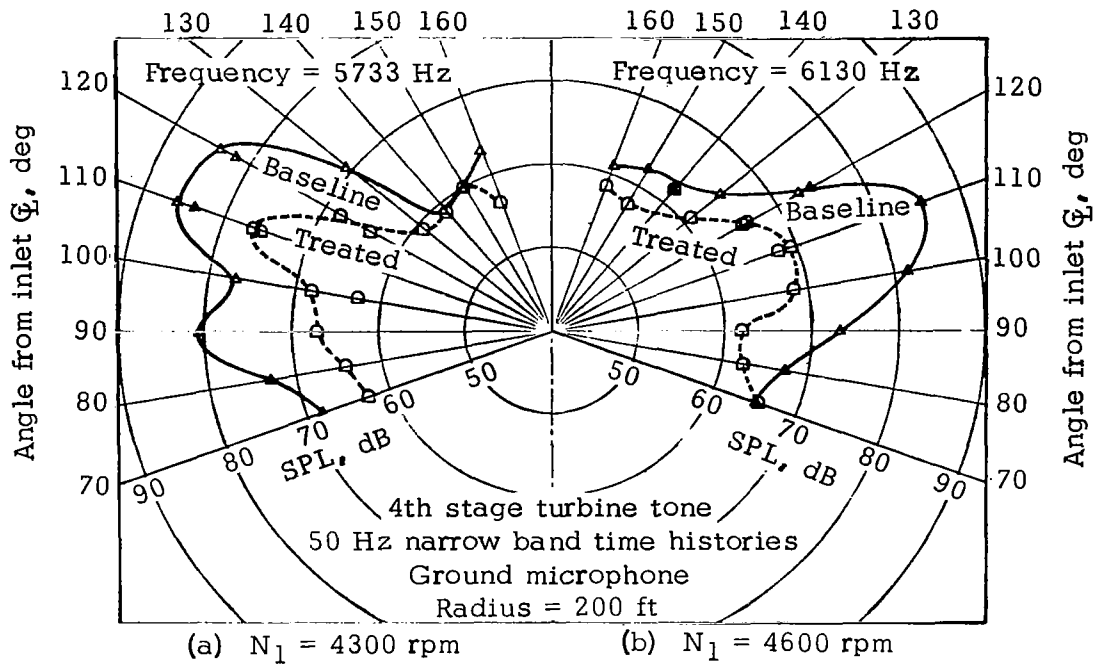


Figure 33. Effect of higher approach power conditions on 4th stage turbine tone suppression

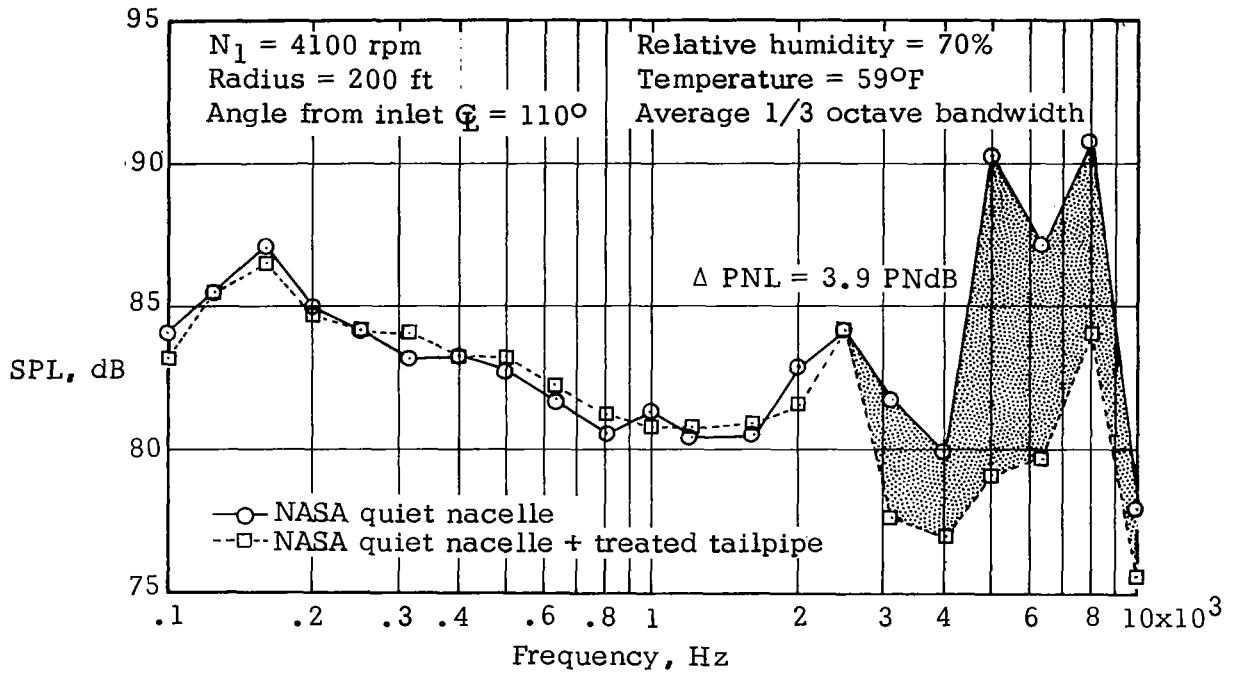


Figure 34. Tailpipe noise comparison at approach power

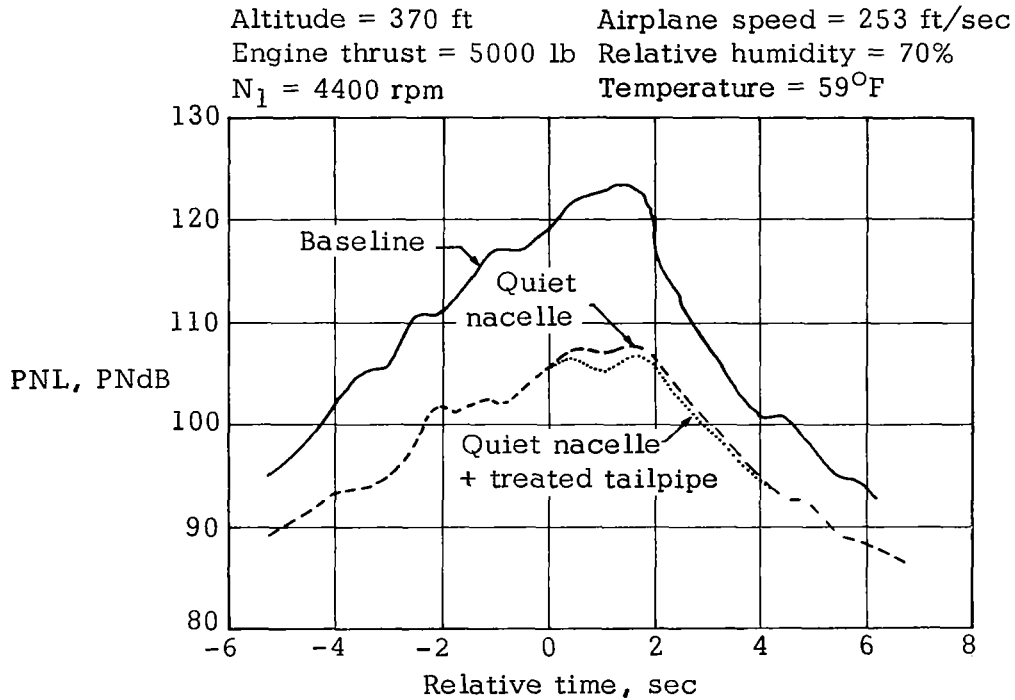


Figure 35. Perceived noise time history during landing approach

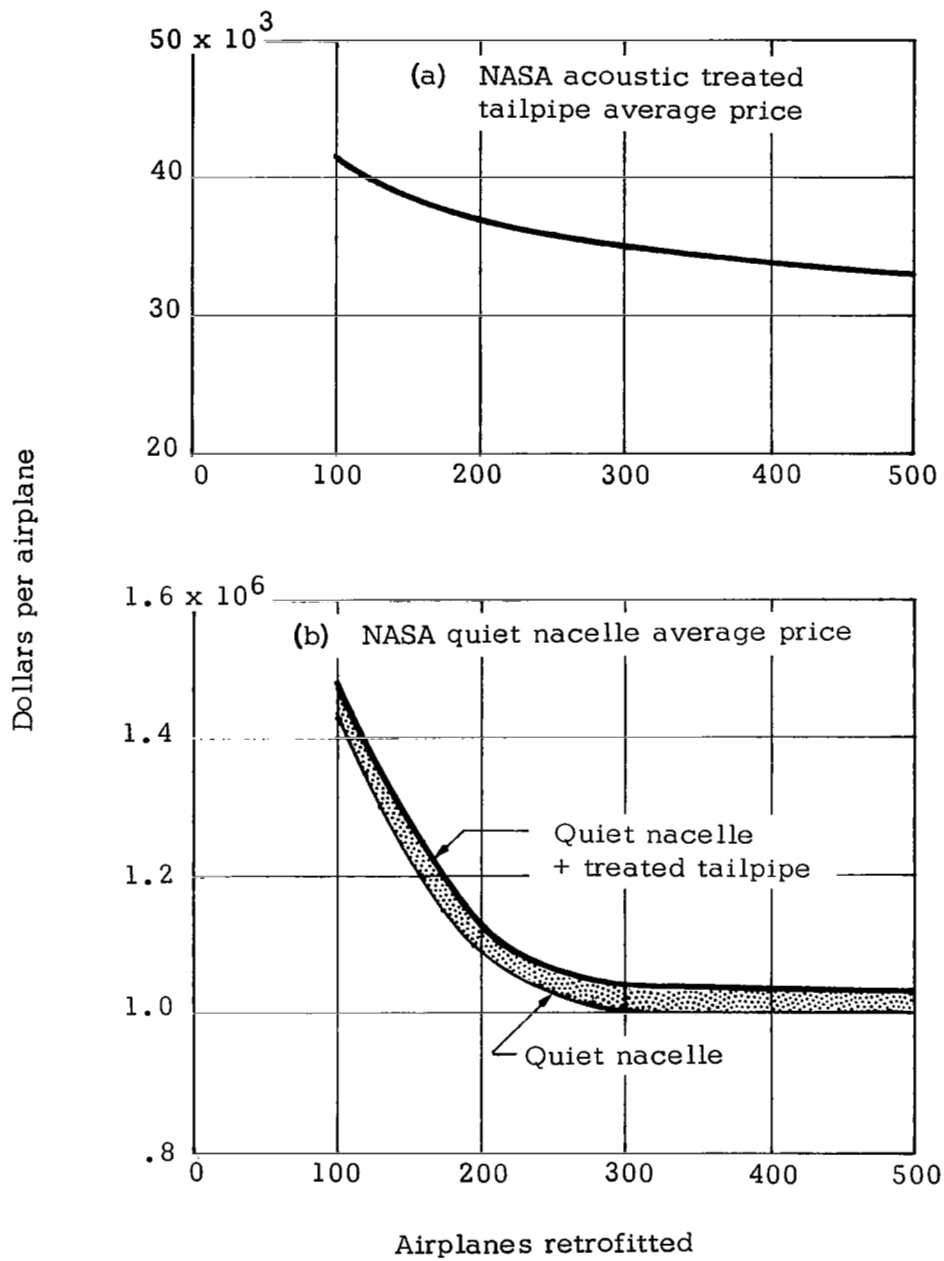


Figure 36. NASA quiet nacelle average price comparison

APPENDIX

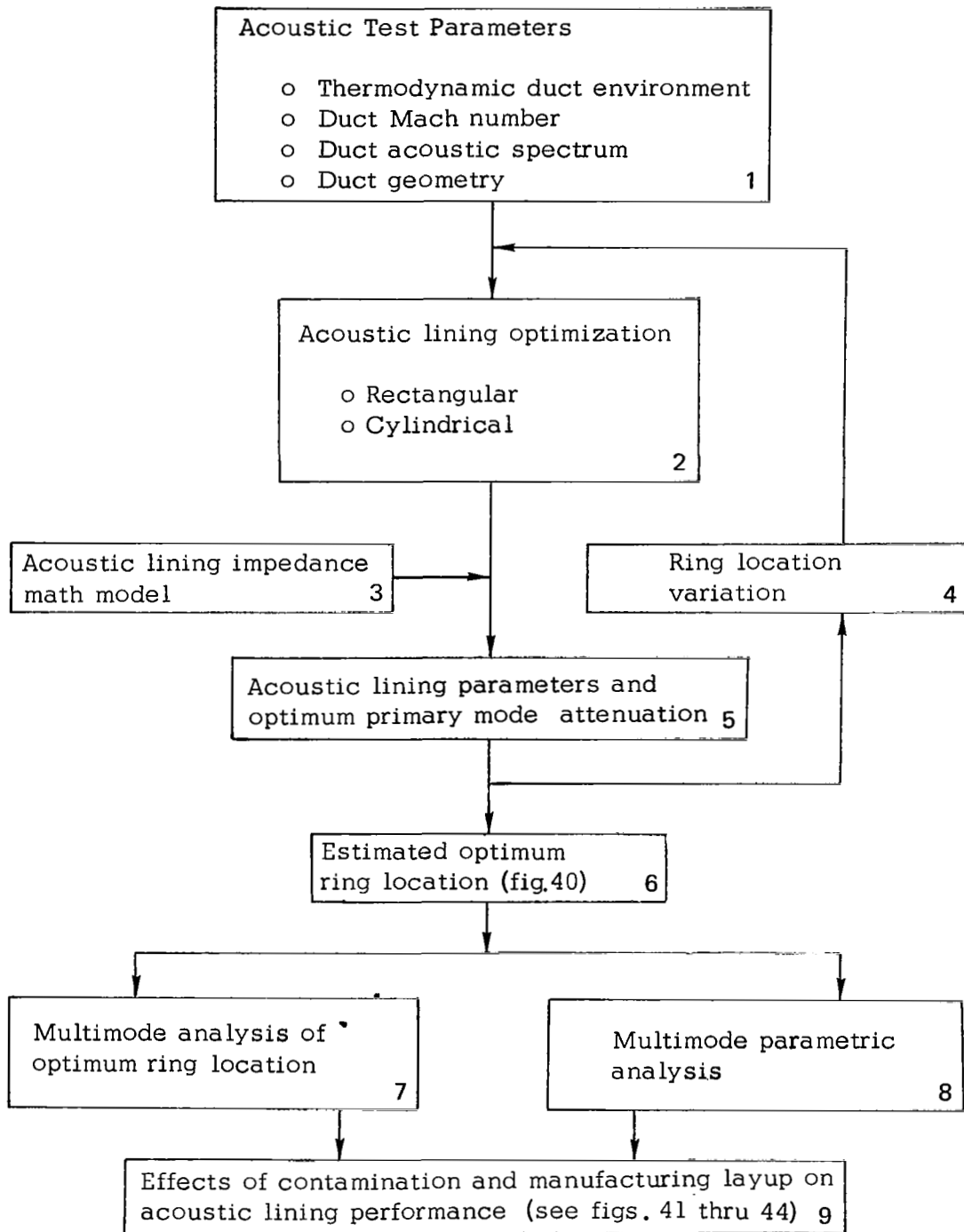


Figure 37. Acoustic lining design analysis procedure

APPENDIX

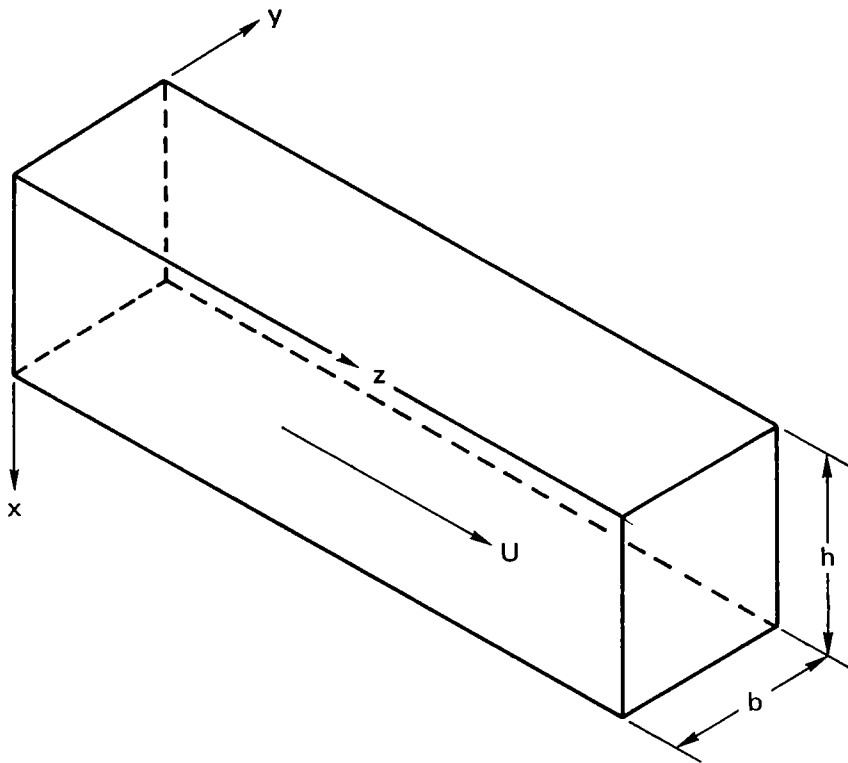


Figure 38. Geometry of duct

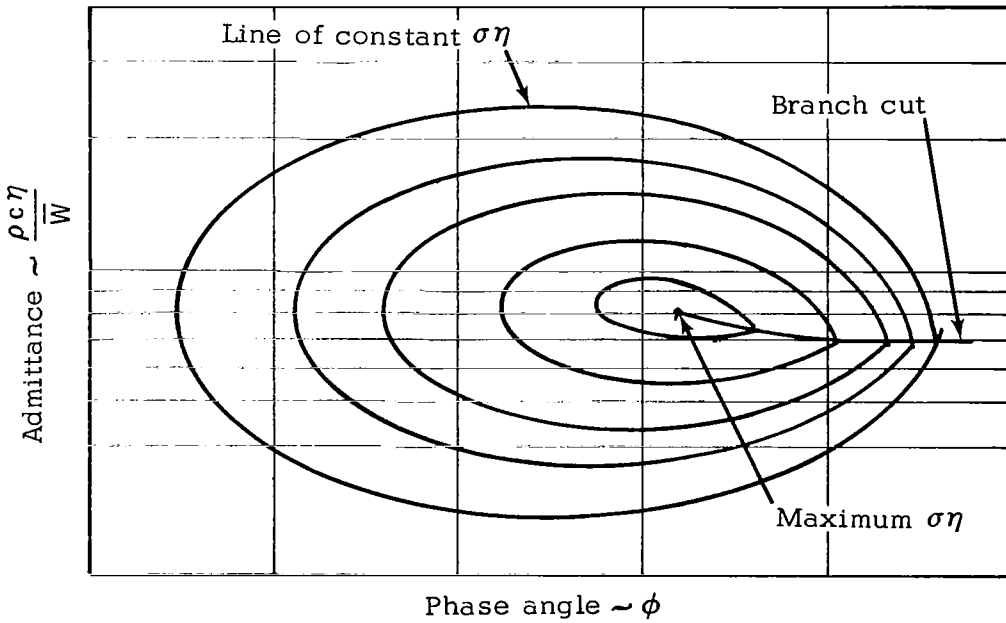


Figure 39. Optimum admittance determination

APPENDIX

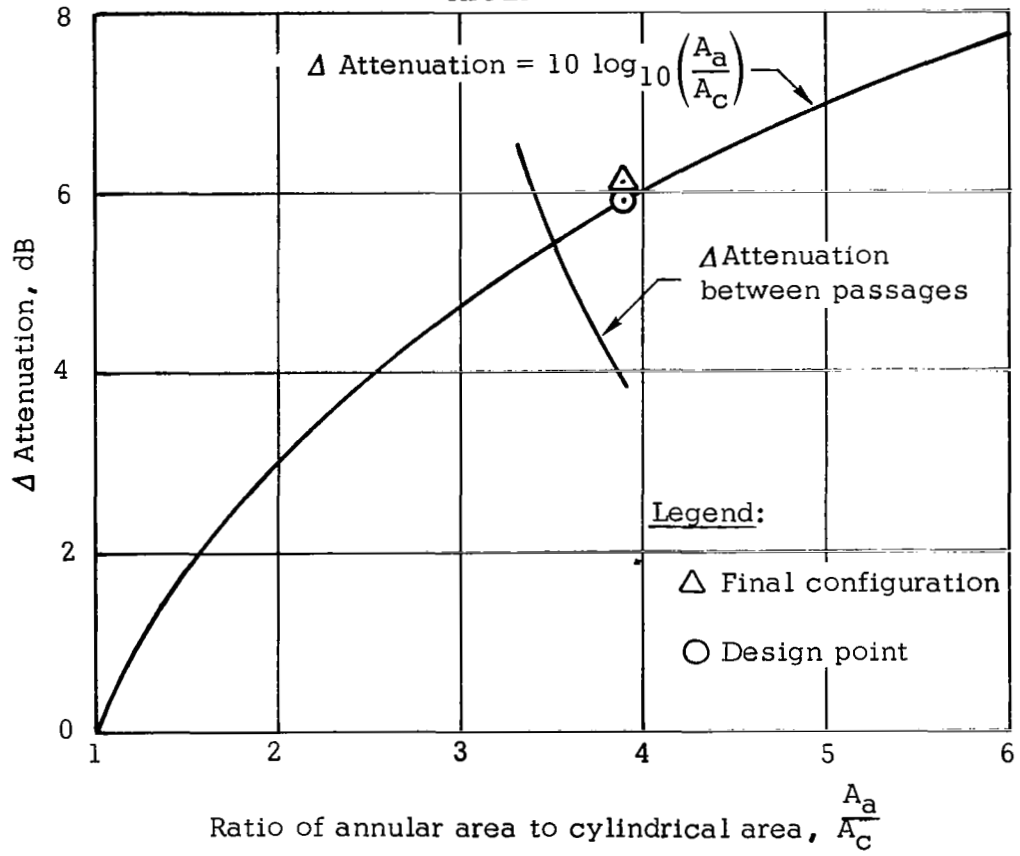


Figure 40. Optimization of acoustic ring placement

APPENDIX

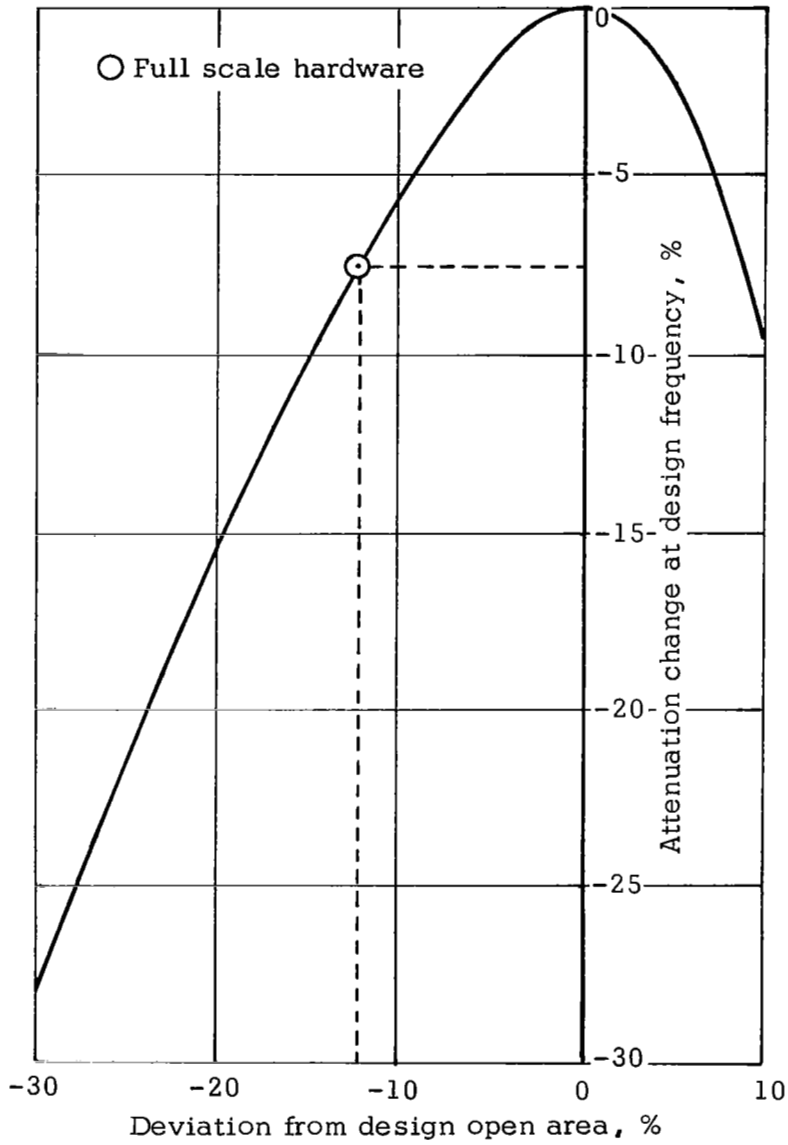


Figure 41. Face sheet blockage trades based on design frequency

APPENDIX

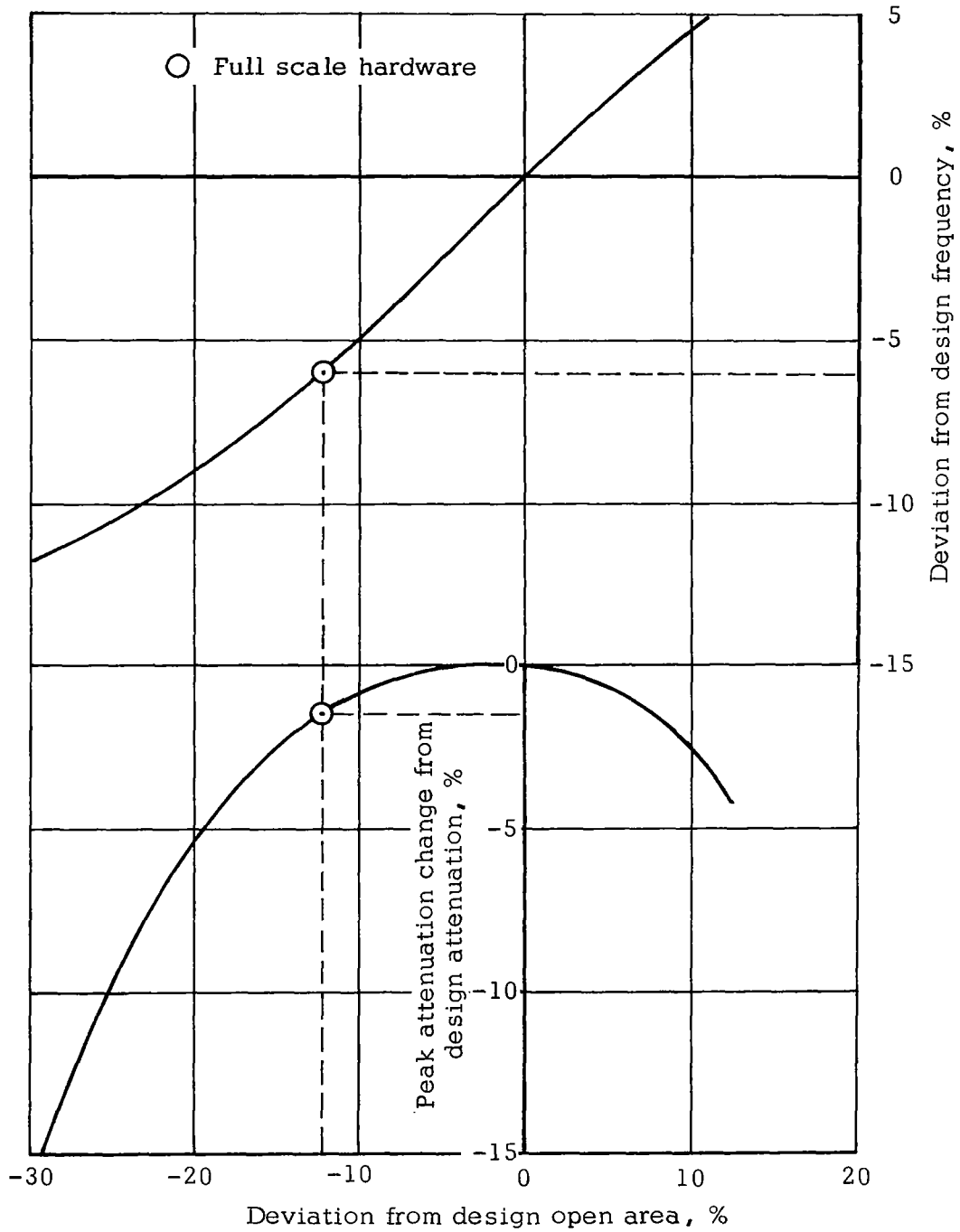


Figure 42. Face sheet blockage trades based on peak attenuation frequency

APPENDIX

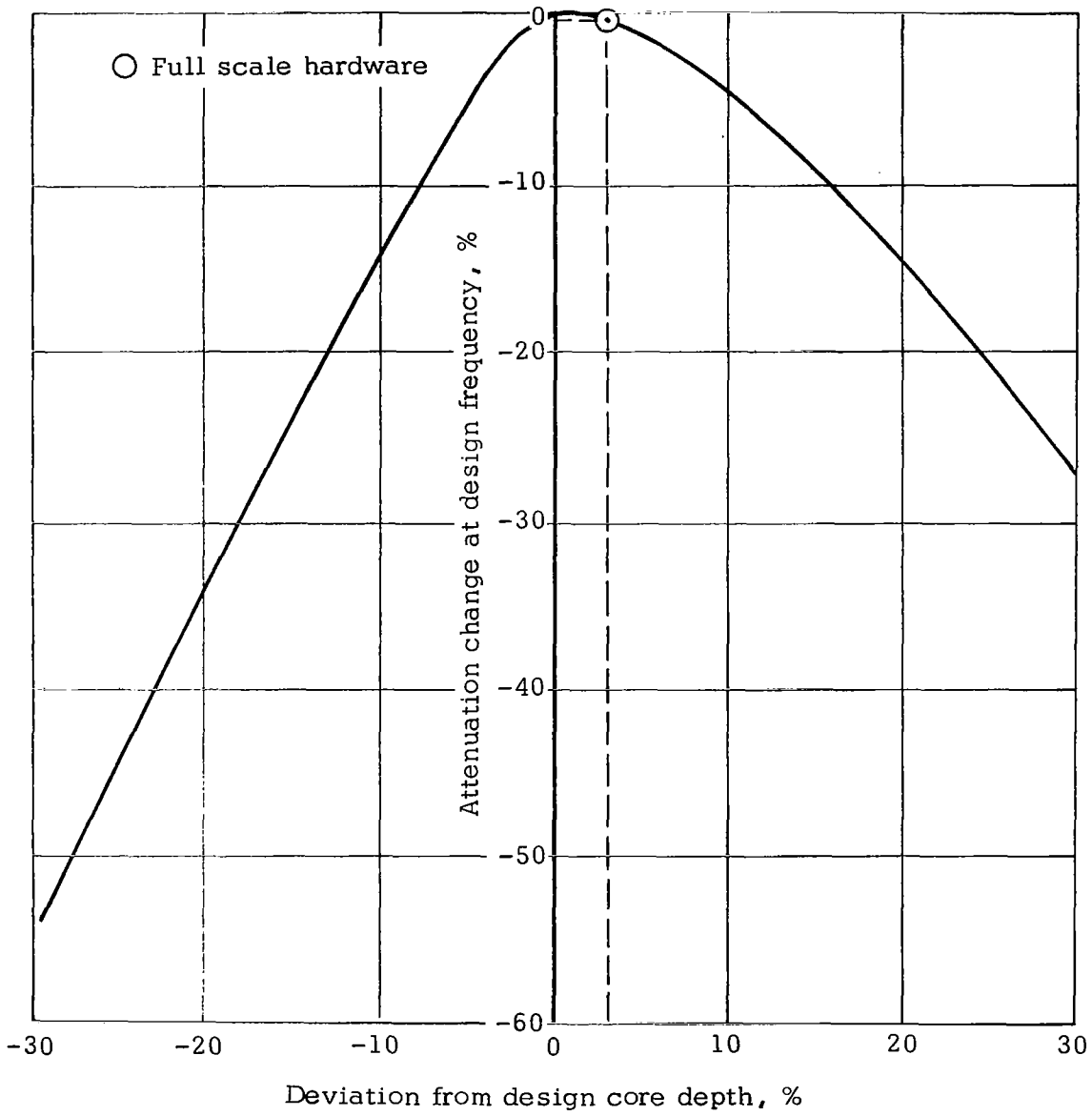


Figure 43. Core depth variation trades based on design frequency

APPENDIX

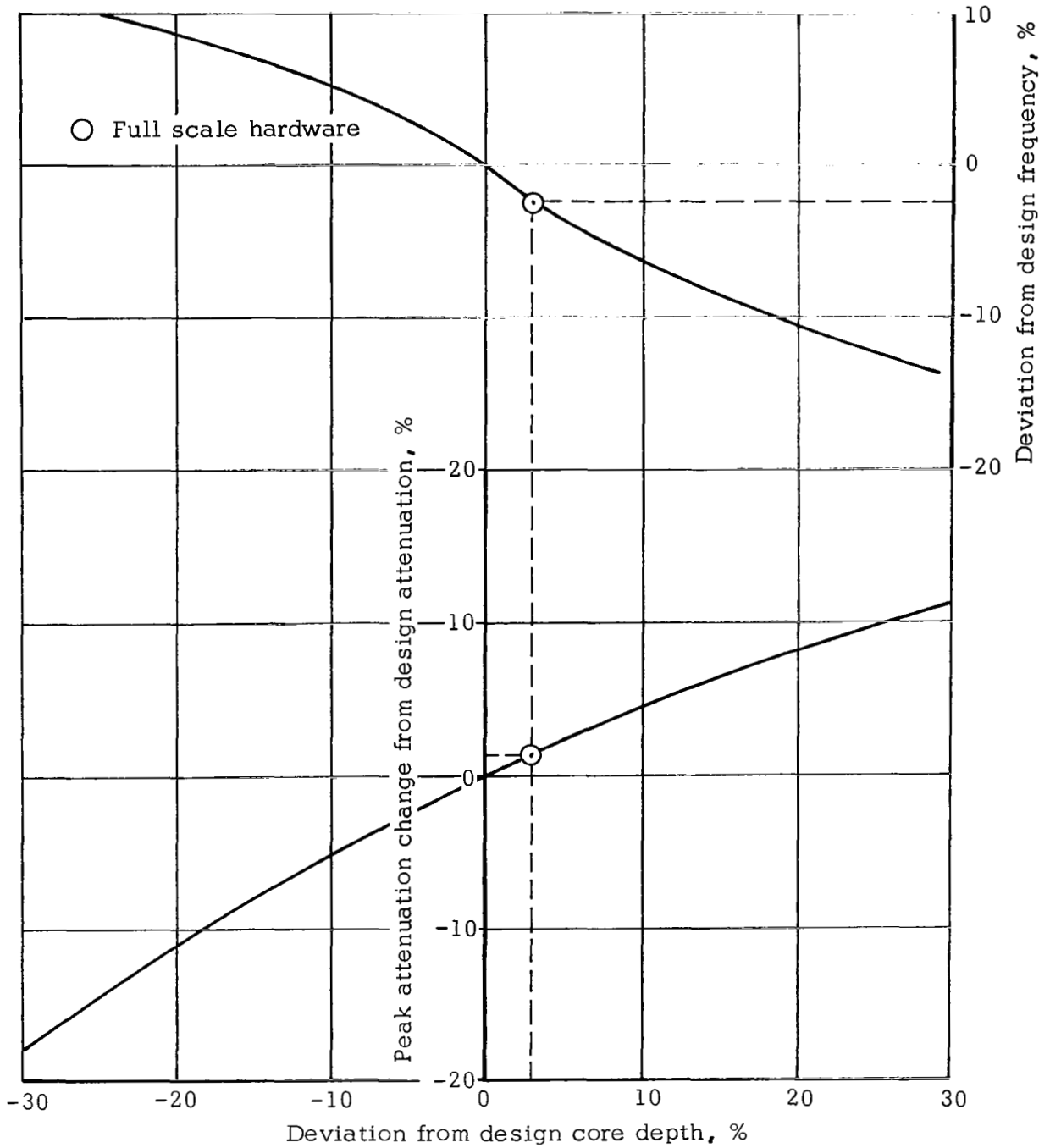


Figure 44. Core depth variation trades based on peak attenuation frequency